© 2021. Published by The Company of Biologists Ltd | Journal of Cell Science (2021) 134, jcs254599. doi:10.1242/jcs.254599

RESEARCH ARTICLE

Control of SRC molecular dynamics encodes distinct cytoskeletal responses by specifying signaling pathway usage

Adèle Kerjouan[1], Cyril Boyault[1], Christiane Oddou[1], Edwige Hiriart-Bryant[1], Alexei Grichine[1], Alexandra Kraut[2], Mylène Pezet[1], Martial Balland[3], Eva Faurobert[1], Isabelle Bonnet[4], Yohann Coute[2], Bertrand Fourcade[3], Corinne Albiges-Rizo[1] and Olivier Destaing[1,*]

ABSTRACT

Upon activation by different transmembrane receptors, the same signaling protein can induce distinct cellular responses. A way to decipher the mechanisms of such pleiotropic signaling activity is to directly manipulate the decision-making activity that supports the selection between distinct cellular responses. We developed an optogenetic probe (optoSRC) to control SRC signaling, an example of a pleiotropic signaling node, and we demonstrated its ability to generate different acto-adhesive structures (lamellipodia or invadosomes) upon distinct spatio-temporal control of SRC kinase activity. The occurrence of each acto-adhesive structure was simply dictated by the dynamics of optoSRC nanoclusters in adhesive sites, which were dependent on the SH3 and Unique domains of the protein. The different decision-making events regulated by optoSRC dynamics induced distinct downstream signaling pathways, which we characterized using time-resolved proteomic and network analyses. Collectively, by manipulating the molecular mobility of SRC kinase activity, these experiments reveal the pleiotropy-encoding mechanism of SRC signaling.

KEY WORDS: SRC, Conformational intermediates, Optogenetics, Time-resolved phosphoproteomics, Pleiotropy, Migration, Invasion, Encoding intracellular signaling, Cytoskeletal, Adhesions

INTRODUCTION

Numerous extracellular stimuli are integrated by multiple receptors that activate a limited number of intracellular multi-domain signaling molecules that coordinate cell responses. How specific cellular responses are generated through precise control of the spatio-temporal dynamics of activation of a particular signaling molecule has remained a fundamental open question.

To investigate this paradigm, we focused on the first discovered proto-oncogene, c-SRC (used here to refer to the wild-type endogenous SRC protein). Each member of the SRC family kinases (SFKs) is highly pleiotropic, regulating diverse cellular outputs such as metabolism, proliferation, gene expression and cell morphology (Parsons and Parsons, 2004). The ability of c-SRC signaling to decide between distinct cellular responses regulating adhesions and cytoskeletal remodeling clearly sustains its role in decision making during migration and invasion processes (Boateng and Huttenlocher, 2012). c-SRC can even generate antagonistic responses in acto-adhesive structures such as invadosomes, being essential for both their assembly and dismantling (Destaing et al., 2008). Consequently, decrypting the numerous potential c-SRC signaling activities in these dynamic acto-adhesive structures is challenging, as these activities occur at micrometer and minute spatio-temporal scales.

To investigate the mechanism of SRC encoding activity, we need to dynamically integrate all structural elements that allow c-SRC to sample inputs, to route specific signaling pathways among a large repertoire and to encode specific cellular phenotypes. The pleiotropy of SFK members is supported by their canonical structure, in which their kinase domain is targeted to membranes by an SH4 domain and maintained fully closed by two intramolecular interactions: one between the SH2 domain and a C-terminal phosphorylated tyrosine, and the second between the SH3 domain and an internal proline rich region (PRR; Young et al., 2001). Release of these intramolecular interactions fully activates c-SRC kinase activity through the opening of its bi-lobal kinase domain and provoking a cascade of events: autophosphorylation of the Y416 residue (Roskoski, 2015) and solvent exposure of the adaptor SH3, PRR and SH2 domains, as well as the C-terminal phosphorylated tyrosine, which all become available for extramolecular interactions. Therefore, the tight coupling between enzymatic activation and adaptor functions modulates the duration and level of SRC kinase activity (Bernadó et al., 2008).

Given the structural complexity of c-SRC, one can predict that c-SRC signaling is not based on a simple binary activation but instead relies on the relationship between a multitude of possible c-SRC conformational intermediates defined by combinations of inter-domain interactions (Fig. 1A,B). Interactions with lipids add an additional layer of complexity by affecting the binding capacities of the poorly structured Unique domain (UD) and SH3 domain (Pérez et al., 2013). Finally, the level of clustering and oligomerization, from the poorly known c-SRC dimers to 80-nm nanoclusters of c-SRC molecules, also contributes to complexity in SRC signaling (Irtegun et al., 2013; Smith et al., 2016; Spassov et al., 2018). The numerous possible SRC conformational intermediates suggests that the pleiotropy of c-SRC signaling emerges from a heterogeneous population of molecules with different levels of kinase activity that dynamically targets a repertoire of interactors.

Understanding the functional relevance of these multiple c-SRC conformational intermediates in a dynamic manner is impossible with classical genetic methods (Fig. 1A). Optogenetic manipulations have emerged as a powerful tool to dynamically regulate cell signaling (Toettcher et al., 2013). Nevertheless, with a

[1]Institute for Advanced Biosciences, Centre de Recherche Université Grenoble Alpes, Inserm U 1209, CNRS UMR 5309, 38706 La Tronche, France. [2]Laboratoire EDYP, BIG-BGE, CEA, 38054 Grenoble, France. [3]Laboratoire Interdisciplinaire de Physique (Liphy), Université Grenoble Alpes, CNRS, 38000, 38402 Saint-Martin-d'Héres, France. [4]Laboratoire Physico-Chimie Curie, Institut Curie, PSL Research University, Sorbonne University, UMR 168, 75005 Paris, France.

*Author for correspondence (olivier.destaing@univ-grenoble-alpes.fr)

I.B., 0000-0003-2343-3784; Y.C., 0000-0003-3896-6196; O.D., 0000-0001-7622-3700

Handling Editor: Michael Way
Received 19 October 2020; Accepted 13 November 2020

Journal of Cell Science (2021) 134, jcs254599. doi:10.1242/jcs.254599

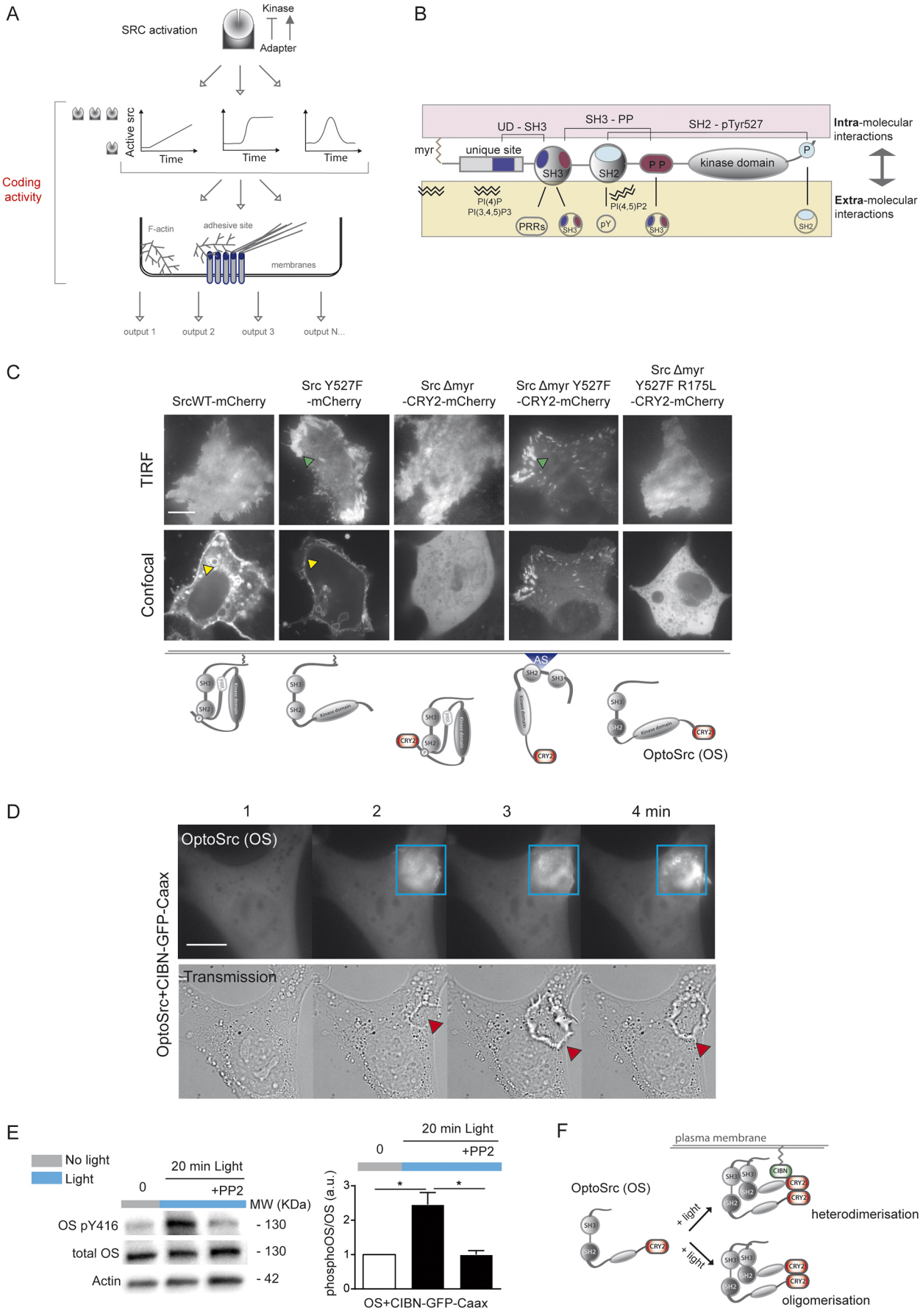

Fig. 1. See next page for legend.

Journal of Cell Science

Journal of Cell Science (2021) 134, jcs254599. doi:10.1242/jcs.254599

Fig. 1. Optogenetic control of the non-receptor tyrosine kinase SRC. (A) Schematic of how coupled adaptor and kinase activities of SRC could trigger different cellular outputs. (B) A large number of combinations of SRC conformation is sustained by numerous intra- and extra-molecular interactions [between the myristoylated domain (myr) and unique site (UD), UD and SH3 (UD-SH3), SH3 and the prolin-rich region (SH3-PP), and SH2 and phosphotyrosine (SH2-pTyr527)]. (C) Top: representative images of different optogenetic probes engineered and expressed in MDCK cells maintained in the dark, which led to development of optoSrc (OS) – a potentially active tyrosine kinase that is fully cytosolic while not localized in ECM adhesive sites (green arrows) and cell-cell contacts (yellow arrows). Bottom: diagrams showing the conformation of endogenous c-SRC, the active SRC mutant Y527F and the different optogenetic probes (fused with CRY2) associated with membranes or binding adhesive sites (AS). (D) Representative time series showing that local cyclic activation of OS (blue square, 100 ms pulse every 30 s over 5 min) induces recruitment to the plasma membrane of fibroblasts expressing CIBN–GFP–Caax, triggering large dorsal ruffles locally (red arrows). (E) Light-dependent recruitment of OS to the plasma membrane of MDCK cells expressing CIBN–GFP–Caax induces SRC-dependent activation of its kinase domain (measured by OS pY416:total OS ratio), which is inhibited in the presence of PP2. Actin is shown as a loading control. Data are shown as mean±s.e.m.. **P*<0.05 (unpaired, two-tailed Mann–Whitney test). (F) OS photostimulation can lead to either its membrane relocalization (through heterodimerization with membrane-anchored CIBN) or its oligomerization. Scale bars: 5 µm.

temporal resolution ranging from 3 to 300 s and a spatial resolution limit of greater than 5 µm (Valon et al., 2015), it remains challenging to access the higher spatial resolution necessary to control acto-adhesive structures. Chemogenetics has been used to directly control the activity of SRC but without achieving both minute-scale and reversible control of SRC at the subcellular level (Chu et al., 2014; Garske et al., 2011), whereas optogenetics was only used to obtain reversible and subcellular photo-inhibition of SRC signaling (Dagliyan et al., 2016).

To spatio-temporally activate and control SRC signaling, we engineered a new photoactivable SRC kinase, optoSRC (OS), based on the CRY2 optogenetic module. By only modulating the mobility of OS nanoclusters in adhesive sites, we were able to generate very different SRC-dependent acto-adhesive structures – lamellipodia and invadosomes – showing that it is possible to induce different decision-making events optogenetically. Indeed, cyclic light-dependent OS oligomerization sustained over time was sufficient to induce SH3- and UD-dependent relocalization to adhesive sites, which could also be modulated by potential membrane association. Modeling of these different dynamics of OS showed that these optogenetic manipulations induced different fluxes of SRC signaling into adhesive sites that engaged distinct downstream signaling pathways, as monitored by time-resolved proteomics of co-purified phosphotyrosine-associated proteins (PY) and analysis of network biology. Collectively, with this synthetic approach, we succeeded in hijacking the fundamental principles of SRC coding activity, suggesting new aspects of SRC regulation in line with observations on the dynamics of its physiological nanoclustering. We demonstrated the causal link between the dynamics of OS oligomers at adhesive sites and SRC decision-making activity for triggering different cellular responses.

RESULTS

Development of a light-inducible SRC kinase

The coupled dynamics of SRC kinase activity and adaptor functions have highlighted that the large repertoire of possible c-SRC conformations supports the complexity of its signaling activity (Fig. 1A). Owing to the numerous possible intra- or extra-molecular interactions (Fig. 1B), it is not clear how spatio-temporal control of c-SRC activity triggers different cellular responses (Fig. 1A,B). Precise spatial control of c-SRC activation is important for acto-adhesive structures, such as lamellipodia or invadosomes (Fig. S1A).

Besides trying to reproduce the complexity of endogenous activation of SRC, we developed a CRY2-dependent optogenetic system (Kennedy et al., 2010) to spatio-temporally control its activity. This synthetic tool was based on reported SRC mutations that affect both c-SRC membrane localization and the opening of its kinase domain. Our strategy was to create a potentially active and cytosolic SRC mutant displaying SRC signaling events only upon light stimulation while being maintained in an inactive state in the dark. Thus, the CRY2–mCherry module was fused to a SRC mutant with a deleted membrane-anchoring domain (SRCΔmyr–CRY2–mCherry), leading to an absence of localization in cell–cell contacts or adhesive sites of Madin–Darby canine kidney (MDCK) cells that was distinct from the localization of mCherry-tagged wild-type (WT) c-SRC (SRCWT–mCherry) or the active mutant SRC Y527F–mCherry (Fig. 1C). This mutant was made potentially active by opening its closed conformation through the substitution of phenylalanine at the regulatory Y527 residue. Despite not accumulating at cell–cell contacts, the SRCΔmyr Y527F–CRY2–mCherry mutant was able to localize to adhesive sites in the dark (Fig. 1C). An additional point mutation, R175L, inhibited the PY-binding activity of the SH2 domain and abolished the ability of SRCΔmyr Y527F–CRY2–mCherry to localize to adhesive sites. This final construct, named optoSRC (OS; SRCΔmyr R175L Y527F–CRY2–mCherry mutant) did not accumulate in any cellular compartment in the dark (Fig. 1C).

The functionality of OS was validated by assessing the induction of a typical SRC-driven cellular response by light upon its membrane relocalization. OS relocalization was obtained through CRY2 heterodimerization with a plasma membrane-anchored CIBN (CIBN–GFP–Caax) in response to local light stimulation (Fig. 1D). As expected for CRY2–CIBN heterodimerization, sustaining cyclic light stimulation (100 ms stimulation every 30 s over 10 min) induced periodic OS membrane localization with a 5 µm spatial resolution (Fig. S1B). Local membrane recruitment of OS provoked the rapid formation of large dorsal ruffles (Fig. 1D; Movie 1) and phenocopied the effects of expression of a constitutively active mutant of SRC (SRC Y527F; Fig. S1C) as well as the activation of thermosensitive and chemo-activable SRC mutants (Mettlen et al., 2006; Gentry et al., 2016). The physiological relevance of OS was further confirmed by comparing its ability to activate ERK pathways (here referring to ERK1 and ERK2, also known as MAPK3 and MAPK1, respectively) in the same range as physiological stimuli such as EGF stimulations or cell spreading on different extracellular matrices (Fig. S2). The light-dependent membrane recruitment of OS was associated with self-activation of its kinase domain, as indicated by PP2-sensitive auto-phosphorylation of its Y416 residue (Fig. 1E). Furthermore, the specific light-dependent activation of OS and the low leakiness of OS in the dark was confirmed by analyzing paxillin (PXN) phosphorylation, the main cytosolic substrate of c-SRC (Fig. S1D).

Taken together, our data show that OS is a fully functional optogenetic SRC system mimicking numerous physiological SRC functions.

Different activation of OS encodes distinct phenotypic acto-adhesive responses

The ability of CRY2 to oligomerize was used to induce SRC nanoclusters (Fig. 1F), whose *in vivo* functions are poorly

Journal of Cell Science (2021) 134, jcs254599. doi:10.1242/jcs.254599

characterized. Since CRY2 oligomerization and CRY2–CIBN heterodimerization co-exist (Duan et al., 2017), we tested whether anchoring OS nanoclusters at the membrane or not would affect their ability to induce different signaling events. To compare signaling activity of OS nanoclusters associated or not with membranes (depending on CIBN–GFP–Caax expression), and because SRC signaling occurs at cell–matrix adhesions, we used blue TIRF excitation to induce nanoclusters in the vicinity of the plasma membrane. TIRF blue light cyclic stimulation was sustainably applied on MDCK cells stably co-expressing OS with either CIBN–GFP–Caax (OS+CIBN–GFP–Caax) or GFP–Caax (OS+GFP–Caax). Recruitment of OS oligomers to membrane (OS+CIBN–GFP–Caax) induced characteristic lamellipodia (Fig. 2A; Movie 6) that were rarely present in epithelial MDCK cells. Lamellipodia were highly sensitive to OS activation, because they rapidly formed after OS activation and disappeared only 5 min after the end of photostimulation (Fig. 2A kymograph). These light-induced lamellipodia were not specific to OS nanocluster recruitment to Caax, but rather were dependent on OS recruitment on the plasma membrane in general, because they were also observed upon expression of the endogenous anchoring domain of SRC (myr–GFP–CIBN; Fig. S3A). Surprisingly, formation of OS nanoclusters in the cytosol (OS+GFP–Caax) induced large, curved, auto-assembling centrifugal actin rings after sustained cyclic photostimulation (33 mHz; Fig. 2B; Movie 5). These structures were invadosome rings, as characterized by their stereotypical auto-assembling behavior, OS localization and accumulation of LifeAct–iRFP (Fig. 2B) and cortactin (Fig. 2C). Activation of the kinase-dead OS mutant (OS-K295M) or PP2 pre-treatment before induction of OS oligomerization abolished invadosome formation, demonstrating the need for Src kinase activity for their formation (Fig. S3B,C). Interestingly, both of these acto-adhesive structures implicated in migration or invasion are poorly present in epithelial MDCK cells. Quantitative analysis confirmed that cytosolic OS oligomers essentially induced invadosome formation but poorly induced lamellipodia, whereas recruitment of OS oligomers to the membrane essentially induced lamellipodia and dorsal ruffles (Fig. 2D). Therefore, the two types of OS oligomer dynamics (membrane or cytosolic diffusion) clearly gave rise to different cellular responses. Accordingly, with the same photostimulation frequency, lamellipodia were formed immediately after OS activation (1 min±0.5 min; mean±s.d.), whereas invadosome appearance needed longer and sustained stimulation (15.6 min±10 min). The choice of the frequency of cylic light stimulation was adapted based on the endogenous 5 min reversion rate of activated CRY2 in order to induce or not a cumulative trend of activated optoSRC (Fig. S1B, Fig. S4F). As described previously (Valon et al., 2015), this strategy allowed modulation of the quantity of activated OS molecules by applying different frequencies of light stimulation over the same duration (around 20 min), and thus facilitated testing of the relationship between the quantity of OS oligomers and the sensitivity of each cellular response. In marked contrast to lamellipodia induction, which was apparent for all frequencies tested (Fig. 2F), invadosomes were not able to form if the flux of OS oligomers was not sufficient (requiring photostimulation at a frequency greater than 2 mHz; Fig. 2E), confirming the importance of sustaining formation of OS oligomers over time to induce this type of structure.

Our data showed that both duration and quantity of activated OS molecules can be controlled optogenetically and can give rise to different and specific SRC-dependent acto-adhesive structures in cells not forming them classically. Surprisingly, without membrane association, OS oligomerization itself is sufficient to induce highly SRC-sensitive structures such as invadosomes. In conclusion, we were able to directly manipulate SRC pleiotropy and encode different cellular phenotypes by simply modulating SRC oligomer dynamics.

OS nanoclustering drives its own relocalization to adhesive sites

The striking signaling effect of OS oligomers on invadosome formation raised the question of the functionality and localization of these signaling nanoclusters. Firstly, we compared OS oligomerization with observed physiological SRC nanoclusters (2–10 molecules; Smith et al., 2016). To characterize the oligomerization level of light-activated OS in our conditions, we measured the variations of OS molecular brightness, which are proportional to the oligomerization status of a fluorophore (Digman et al., 2008), using fluorescence correlation spectroscopy (FCS). Activated OS presented a significant increase in brightness that became comparable to the brightness of two OS that were molecularly fused (double OS) and maintained in the dark (Fig. S4A). This indicates that activated OS can form small oligomers (from dimers to low-order oligomers).

We used cyclic blue light TIRF illuminations (100 ms stimulation every 30 s over 10 min) to induce mostly OS oligomers in the vicinity of the plasma membrane. Surprisingly, formation of OS oligomers induced their rapid and specific relocalization from the cytosol to adhesive sites, as they colocalized with the focal adhesion markers vinculin, p130CAS (also known as BCAR1) and paxillin (Fig. 3A,B; Fig. S4D, Movie 2) but not with clathrin or caveolin sites, which are other c-SRC-sensitive plasma membrane-targeted loci (Fig. S4B). This relocalization was not dependent on oligomerization with endogenous SFK members because it was still effective in SYF cells (*c-Src*$^{-/-}$ *Yes*$^{-/-}$ *Fyn* $^{-/-}$cells; Fig. 3C). Light-dependent OS relocalization to adhesive sites was typical of the kinetics of CRY2 activation (activation in a few seconds, reversion in 5 min; Fig. S4F) and thus did not present an obvious difference from OS relocalization at the membrane in the presence of CIBN–GFP–Caax (Fig. S1B). Again, OS expression exhibited poor leakage of its phosphorylation activity under dark conditions, as illustrated by paxillin phosphorylation in MDCK cells and SYF cells (Fig. S5A,B).

Relocalization of OS oligomers to adhesive sites was supported by the SH3 domain functions (Fig. 3D,E; Fig. S4G, Movie 3) as evidenced by its strong decrease upon SH3 deletion (OS-ΔSH3), inhibition of SH3-domain binding to PRR proteins (OS-W118K) or increase of intramolecular SH3-PRR binding (OS-SH3Eng; which has the mutation SRC-K249P/Q252P/T253P; Krishnamurty et al., 2013). In addition, mutation of the internal PRR of OS (OS-PPR-AAA) had no effect on this process (Fig. S4E). Interestingly, the presence of the phosphorylatable Y527 in OS (OS-R175L only) blocked its ability to be relocalized in adhesive sites, showing that Y527 not only controls the kinase domains through the opening of the internal SH2–Y527 bridge but is also implicated in OS partner binding when phosphorylated (Fig. S4C). Light-dependent OS relocalization could either be driven by a simple increase in SH3 local concentration induced by the oligomerization or controlled by a specific SRC-SH3 domain conformation that can be dictated by the vicinity of the SH2 domain and/or tyrosine kinase domain. This last hypothesis was confirmed by the reduced ability of activated OS mutants containing a deleted kinase domain or SH2 domain, or perturbation of the kinase domain (OS-K295M) to relocalize in adhesive sites (Fig. S4D). Finally, reducing clustering properties of CRY2 using the CRY2 low mutant (CRY2-1–488-EED, referred to here as OS LOW; Duan et al., 2017) slightly reduced OS

Journal of Cell Science (2021) 134, jcs254599. doi:10.1242/jcs.254599

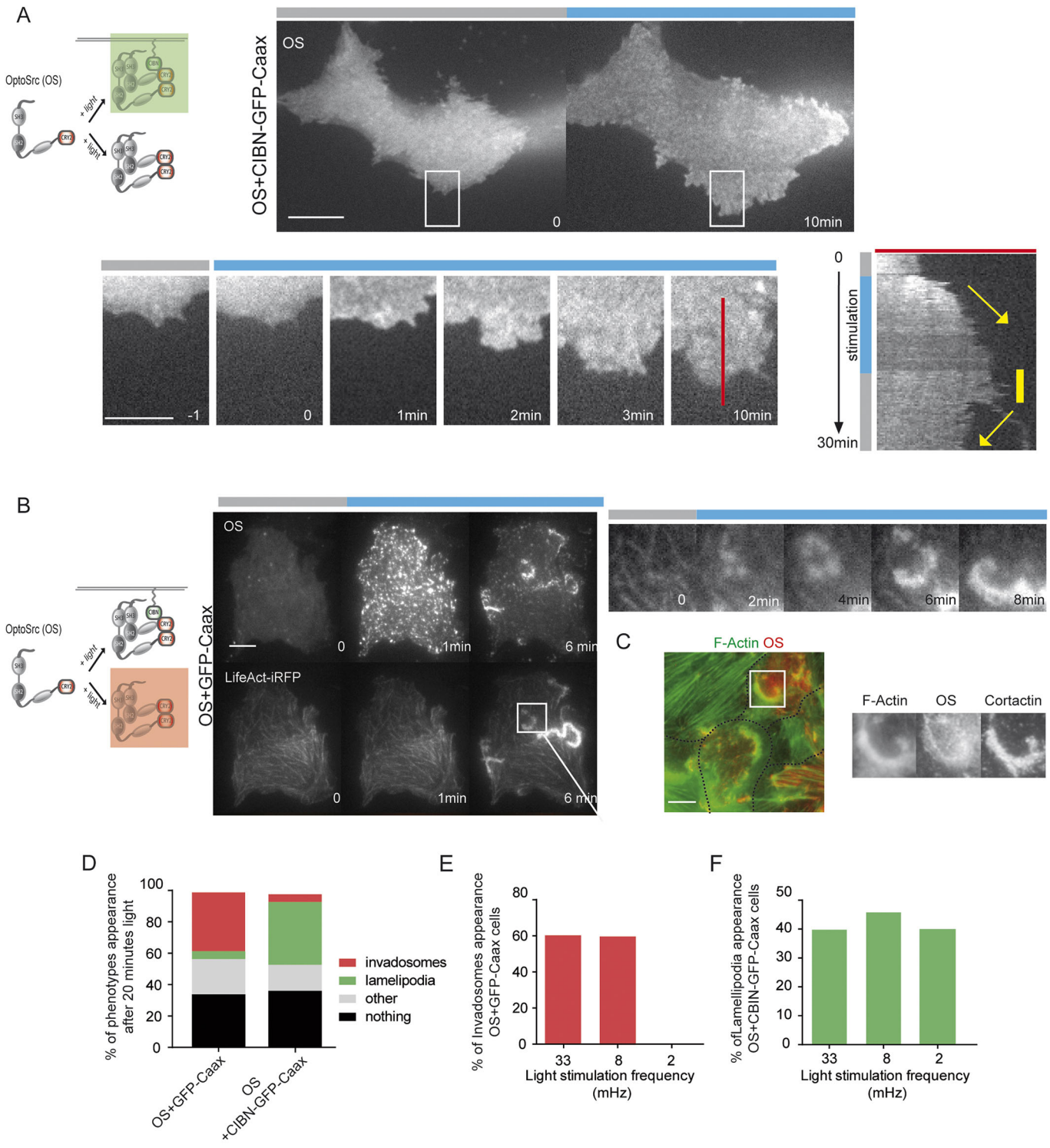

Fig. 2. Different rates of OS molecular flux into adhesive sites generate either lamellipodia or invadosomes. (A) Representative TIRF images (top right) of OS fluorescence illustrating how membrane-associated activated OS oligomers (as shown in the diagram, top left) induce lamellipodia in MDCK cells upon blue light stimulation (blue bars; 50 ms pulse every 30 s over 10 min). White box indicates region shown in time series images (bottom left). Kymograph analysis (bottom right) of a line section (indicated in red in the time series image) showed high dependency of lamellipodia on blue light stimulation. Yellow arrows indicate protrusive lamellipodia (during stimulation) and retracting lamellipodia (no stimulation); yellow bar indicates stable lamellipodia (just after stopping stimulation). (B) Representative TIRF time series (middle) illustrating how activated OS oligomers (as depicted in the diagram on the left) induce dynamic invadosome rings (visualized using LifeAct–iRFP) in MDCK cells upon blue light stimulation (50 ms pulse every 30 s over 10 min). White box indicates the region shown in the enlarged LifeAct–iRFP images on the right. (C) These OS-dependent F-actin rings (visualized using Alexa488–phalloidin) accumulate the invadosome marker cortactin (as assayed using confocal imaging). White box indicates region shown on the right as separate signals. Dotted lines indicate cell outlines. (D) Quantification of the different acto-adhesive phenotypes obtained after 20 min of cyclic blue light stimulation of MDCK cells stably expressing OS with either CIBN–GFP–Caax or GFP–Caax (N>6; >90 cells per condition). (E,F) Quantification of the percentage of cells forming invadosomes (E) or lamellipodia (F) depending on cyclic blue light photostimulation frequency (50 ms pulse over 20 min; N=4; >30 cells per condition). Scale bars: 5 µm.

Journal of Cell Science (2021) 134, jcs254599. doi:10.1242/jcs.254599

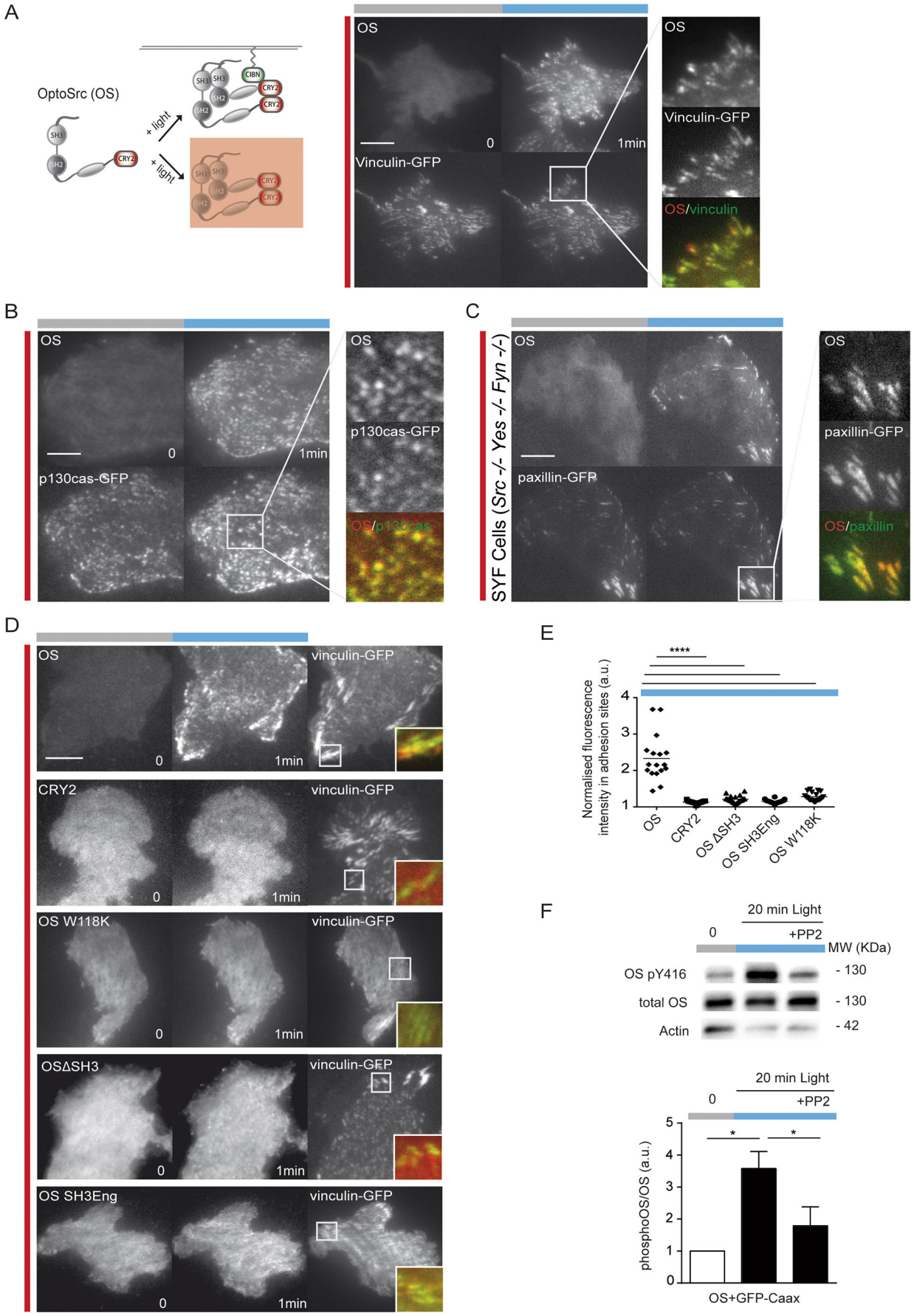

Fig. 3. See next page for legend.

Journal of Cell Science (2021) 134, jcs254599. doi:10.1242/jcs.254599

Fig. 3. Light-dependent OS oligomers relocalize to adhesive sites through their SH3 domains. (A,B) Representative TIRF images before and 1 min after cyclic blue light TIRF photostimulation (blue bars; 50 ms pulse every 15 s) showed relocalization of OS oligomers to adhesive sites of MDCK cells (visualized using vinculin–GFP in A, and p130CAS–GFP in B). (C) Representative TIRF image showing that relocalization of OS oligomers in adhesive sites (visualized using paxillin–GFP) even occurs in SYF cells and thus in the absence of the main endogenous SFKs. (D) Representative TIRF images showing that light-dependent OS oligomer relocalization to adhesive sites of MDCK cells is dependent on its SH3 domains and is not observed for CRY2 alone or OS mutants (OS-ΔSH3, OS-W118K and OS-SH3Eng). White boxes indicate regions shown in inset images for vinculin–GFP. (E) Quantification of OS, CRY2 alone and OS SH3 domain mutants at adhesion sites after blue TIRF photostimulation. Horizontal bar indicates the mean. N=3, >30 cells per condition. ****P<0.0001 (unpaired t-test). (F) Light-dependent oligomerization of cytosolic OS mediates activation of its kinase domain (measured by OS pY416:total OS ratio) through a PP2-sensitive process. Actin is shown as a loading control. Quantification shows mean±s.e.m. of n=4 experiments. Scale bars: 5 µm.

relocalization in adhesive sites without blocking it (Fig. S4C) showing that lower-size oligomers (probably dimers) can support this relocalization.

In addition to regulating OS adaptor functions, we investigated whether SRC nanoclustering also activated OS kinase activity. Light-dependent oligomerization of OS was sufficient to stimulate OS kinase activation, as indicated by an increase of PP2-sensitive Y416 phosphorylation (Fig. 3F), which also occurred in SYF cells (Fig. S5B). This suggests that OS kinase activation is increased by a light-dependent trans-phosphorylation process. Finally, light-induced oligomerization of OS in SYF cells activated its kinase domain and resulted in phosphorylation of paxillin at the same level as that in SYF cells expressing wild-type c-SRC, showing the ability of OS to mimic physiological levels of c-SRC activation (Fig. S5B).

Therefore, controlling oligomerization uncovered the crucial role of the SH3 domain in the functions of SRC nanoclusters – regulating the recognition of specific PRR-enriched proteins in adhesive sites and SRC kinase activation. The light-dependent subcellular relocalization of OS oligomers in adhesive sites demonstrated here is therefore a marked improvement in spatial resolution compared with that of previous CRY2 optogenetics approaches.

Optogenetic control of the different rates of OS recruitment to adhesive sites

In order to explain the different signaling events induced by either OS nanoclusters freely diffusing from the cytosol to adhesive sites or OS nanocluster diffusion at the membrane, we determined the parameters of the dynamics of OS nanocluster recruitment in adhesive sites. First, we determined whether membrane-associated OS oligomers (OS+CIBN–GFP–Caax) could also relocalize to adhesive sites (Fig. 4A; Movie 4). In the presence of CIBN–GFP–Caax, OS oligomers were recruited with the same rate outside (membrane) and inside of adhesive sites (Fig. 4B). By contrast, OS oligomers alone (OS+GFP–Caax) were mainly targeted to adhesive sites (Fig. 4C).

While these two experimental strategies (direct or membrane-based indirect recruitment) both led to sustained OS recruitment to adhesive sites, we compared the rates of OS passing through these sites in terms of quantity and molecular mobility. At the whole basal cell surface, co-expression of CIBN–GFP–Caax allowed recruitment of more OS oligomers at the plasma membrane than when OS was expressed with GFP–Caax (Fig. 4D), probably because of the difference between the large amounts of available membrane-anchored CIBN–GFP–Caax and the small number of adhesive sites. However, OS oligomers were more concentrated in adhesive sites than when associated with membranes (OS+CIBN–GFP–Caax), as revealed by their higher OS:vinculin–iRFP ratio after 10 min of cyclic photostimulation (33 mHz; Fig. 4E). Therefore, these two strategies of OS recruitment generated different densities of OS in adhesive sites over time. In addition to determining the quantity of activated OS in adhesive sites, it was also essential to analyze the molecular mobility of activated OS in both conditions (GFP–Caax or CIBN–GFP–Caax). Thus, we combined optogenetic manipulation with fluorescence recovery after photobleaching (FRAP) analysis to determine the mobility of activated OS molecules in adhesive sites. In comparison to direct recruitment of OS oligomers to adhesive sites, membrane-based indirect recruitment (in the presence of CIBN–GFP–Caax) strongly increased the immobilization of activated OS in adhesive sites (characteristic time of recovery evolving from a mean±s.d. of 8.4±2.6 s to 20.8±8.3 s, associated with a 50% increase of the immobile fraction; Fig. 4F).

Therefore, we were able to generate different quantities and molecular mobilities of activated OS in adhesive sites over time by simply controlling its modes of recruitment.

Next, we characterized the two rates of activated OS recruitment to adhesive sites in response to sustained cyclic light activation using modeling. Our optogenetic system can be schematized as a model in which light activates an OS buffer in the cytosol. Following sustained cyclic photostimulation, this activated buffer (OS*) is flushed either by direct adsorption to the membrane (mimicking the CIBN–GFP–Caax condition) or direct recruitment to adhesive sites (mimicking the GFP–Caax condition; Fig. 4G). A first consequence of this model was a 3D–2D reduction of the dimensionality of the mobility for membrane recruitment of OS* compared with direct adsorption of OS* to adhesive sites, explaining our FRAP results. Indeed, we expected the rate of recovery of OS oligomers in adhesive sites to be greatly reduced for a 2D diffusing membrane-anchored protein (D≈0.2 µm^2 s^{-1}) compared with that for 3D diffusing cytosolic OS oligomers (D≈10 µm^2 s^{-1}; Fig. 4F).

Based on our experimental results, sustained cyclic light activation of OS induces a transport by diffusion of these activated oligomers (OS*) from the cytosol to adsorption sites (composed of receptors for OS*), generating a local diffusion-limited flux of activated OS controlled by the density of receptors composing the sites. To compare both OS* fluxes, numerical simulation was used to compare the early behavior of OS fluxes that were directly recruited to adhesive sites or after a membrane-binding step. As expected, for the same amount of activated OS, this model demonstrated that the flux for direct recruitment of activated cytosolic proteins, $OS^*_{(r,t)}$, to adsorption sites was higher than that for indirect adsorption via membrane binding (Fig. 4H).

This model indicates that both OS dynamics are characterized by both the rate of transport of activated OS and the density of receptors for OS in adsorption sites (Fig. 4G) and predicts that the probability of phosphorylation for any substrates is dependent on both local concentration of OS and residence time of OS. Therefore, controlling the dimensionality of OS oligomer mobility generates different fluxes of OS to adhesive sites that encode different OS signaling events.

Specificities of SRC signaling transfer downstream of different OS dynamics

To understand the causal link between OS dynamics through adhesive sites and decision-making (invadosome versus lamellipodia), we

Journal of Cell Science (2021) 134, jcs254599. doi:10.1242/jcs.254599

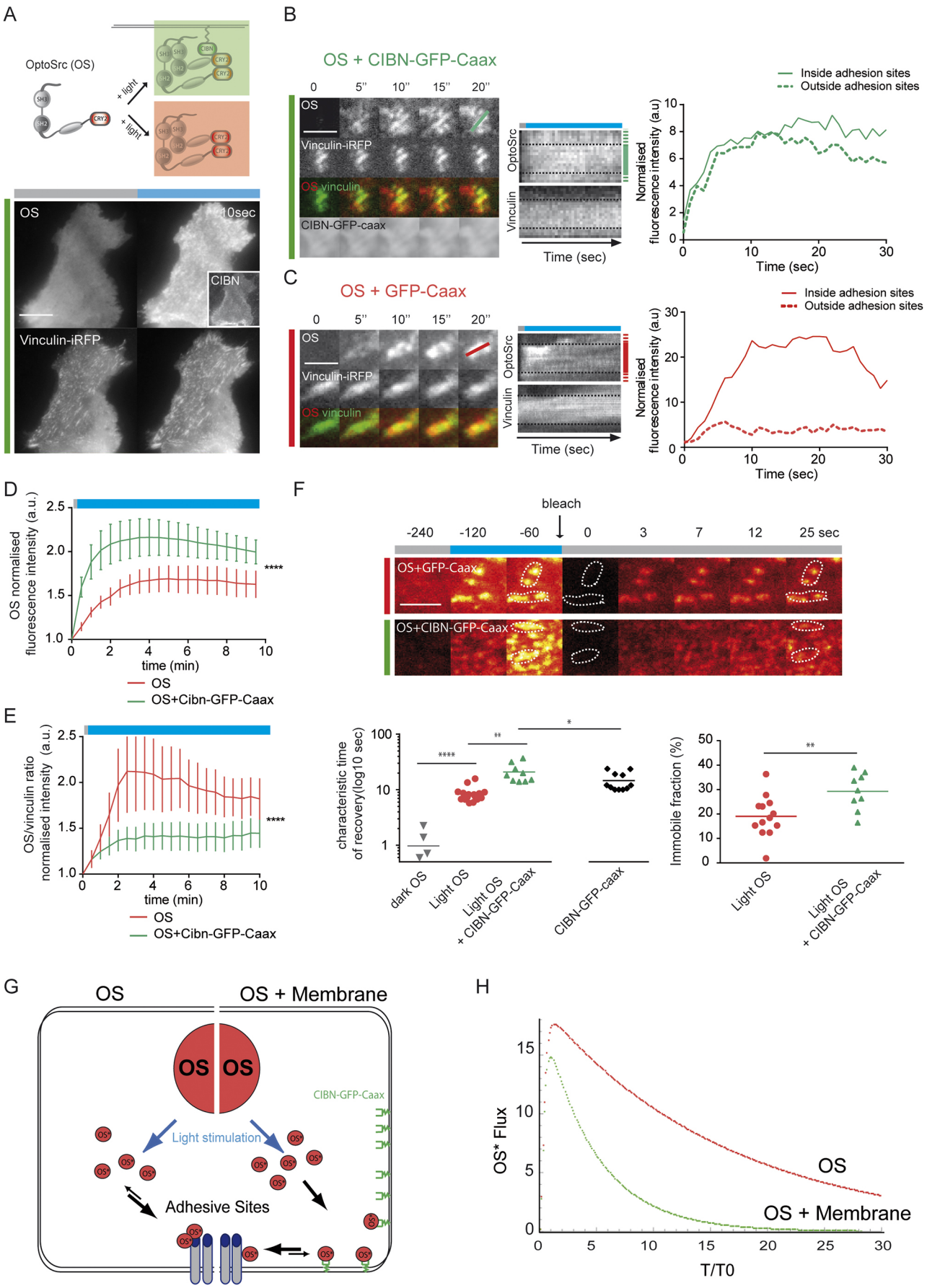

Fig. 4. See next page for legend.

Journal of Cell Science (2021) 134, jcs254599. doi:10.1242/jcs.254599

Fig. 4. Modulation of activated OS molecular flux in adhesive sites by controlling OS membrane anchoring. (A) Top: diagram showing that OS photostimulation can lead to either its membrane relocalization (through heterodimerization with membrane-anchored CIBN, green) or its oligomerization (red). Bottom: representative TIRF images of light-dependent OS oligomer relocalization (red bar, before photostimulation; blue bar, photostimulation) in adhesive sites (visualized using vinculin–iRFP) after membrane recruitment mediated by co-expression of CIBN–GFP–Caax in MDCK cells. (B,C) Time series images (left), kymographs (middle) and quantification (right) of relocalization dynamics in response to TIRF photostimulation (50 ms pulse every 15 s) of OS oligomers inside and outside of adhesive sites when co-expressed in MDCK cells with (B) CIBN–GFP–Caax or (C) the control GFP–Caax. Lines in the time series images indicate the positions of kymograph sections. Dotted lines in kymographs indicate the boundary of vinculin-positive adhesive sites. Graphs shows mean intensities at the level of the representative kymographs inside adhesive sites (plain line) or at the vicinity of adhesive sites but outside of them (dashed line). (D,E) Quantification of OS relocalization at the whole basal level of the plasma membrane (D) or specifically in adhesive sites (E; OS:vinculin–iRFP ratio) after blue light TIRF photostimulation of MDCK cells expressing OS with either CIBN–GFP–Caax (OS+CIBN–GFP–Caax) or GFP–Caax (OS). Data are mean±s.d. of N=3 with >18 cells per condition. ****P<0.0001 (unpaired t-test). (F) Top: representative TIRF time series of OS relocalization to adhesive sites (white dashed lines) after blue light TIRF photostimulation, followed by FRAP experiments. Bottom: quantification of FRAP parameters for the indicated conditions. N=3, >15 cells per condition. *P<0.05; **P<0.01; ****P<0.0001 (unpaired t-test). (G) Physical principles of a cytosolic OS reservoir that can be relocalized to adhesive sites after its photoactivation (OS*, OS oligomers), directly (OS) or through a membrane-binding step (OS+membrane), mimicking GFP–Caax and CIBN–GFP–Caax conditions, respectively. (H) Numerical simulations of the mean flux of OS* per unit length of an adsorbing cluster and over time, directly (red) or through a membrane-binding step (green). Scale bars: 5 µm (A), 2.5 µm (B,C,F).

determined how the modulation of OS molecular turnover affects different downstream signaling pathways. More precisely, we identified and characterized the enrichment dynamics of proteins co-purified by anti-PY affinity after OS activation (referred to as 'OS-sensitive proteins'; Fig. 5A). The combination of OS activation with PY co-immunoprecipitation was feasible, as exemplified by light- and PP2-dependent phosphorylation of known SRC substrates, such as paxillin and p130CAS (Fig. 5B). We scaled up this setup for both OS fluxes (GFP–Caax or CIBN–GFP–Caax conditions), and OS-sensitive proteins were immunoprecipitated from large MDCK populations photostimulated for 5 or 20 min (33 mHz, Fig. 5A). PY-purified proteins were identified by label-free semi-quantitative mass spectrometry, and their fold changes were averaged from three independent experiments and technical duplicates (Table S1). Under non-stimulated conditions (time 0), more than 95% of the identified PY proteins presented the same level of enrichment in non-stimulated MDCK cells co-expressing either OS+GFP–Caax or OS+CIBN–GFP–Caax. OS light activation significantly modulated the enrichment of only a small fraction of PY proteins (90 OS-sensitive proteins out of 506 PY-proteins at time 0; Fig. 5C).

Because OS-sensitive proteins are a presumed mixed population of tyrosine phosphorylated proteins and associated proteins, we evaluated the probability of identifying direct c-SRC substrates from these 90 OS-sensitive proteins by analyzing the presence of known SRC partners and known PY-containing proteins, using stringent *in silico* prediction of phosphorylation by c-SRC and sensitivity towards PP2. All of the OS-sensitive proteins were positive for at least one of these conditions, supporting the presumed high enrichment of SRC substrates in our pipeline analysis (Table S1). Among OS-sensitive proteins, time-resolved PY-proteome analysis identified many classical SRC substrates (e.g. paxillin, p130CAS and tensins; Sawada et al., 2006; Thomas et al., 1995) or SRC substrates identified by phosphoproteomic approaches (ARHGEF5; p120CAS, also known as CTNND1; SGK269, also known as PEAK1; SGK223, also known as PRAG1; EPHB2; Kuroiwa et al., 2011; Leroy et al., 2009; Luo et al., 2008). In addition, gene ontology (GO) analysis showed a significant enrichment for expected functions, such as motility, kinase signaling and small GTPases (Fig. S6A).

We developed a novel pipeline to compare the enrichment of OS-sensitive proteins over time under the two OS flux modes. As previously described (Kubiniok et al., 2017; Olsen et al., 2006), we employed soft clustering based on fuzzy c-means partitioning to analyze temporal enrichment patterns and to cluster proteins based on their enrichment dynamics (three clusters presenting a global increase or decrease in enrichment; Fig. 5D). Comparison of the cluster compositions showed that modulation of OS dynamics affected PY-protein enrichment, most likely reflecting the phosphorylation dynamics of OS substrates. First, modulation of light-activated OS flux to adhesive sites did not change the dynamic phosphorylation behavior for most OS-sensitive proteins that are important signaling relays or acto-adhesive regulators (ARHGEF5, ARHGEF7, MAPK1, PPP1CC, GIT2, tensin3, ITSN2). By contrast, modulation of activated OS flux to adhesive sites was sufficient to significantly change only the amplitude of phosphorylation of key regulators of acto-adhesive structures (SGK223, p130CAS, ASAP2, tensin1; Table S1). Finally, only 37 proteins out of the 90 OS-sensitive proteins showed cluster changes between both OS dynamics conditions.

To integrate dynamic behavior with signaling specificity downstream of each OS flux, we integrated OS-sensitive protein dynamics with a network analysis based on protein–protein interaction public databases. More than 60% of the 90 OS-sensitive proteins were physically linked and defined three main ensembles of signaling nodes implicated in adhesion signaling (Fig. S6B). The first ensemble was composed of many acto-adhesive elements (paxillin, tensin1–3, p130CAS) or regulators (ASAP2, p120CAS, EPHB2, SGK269, SGK223, PPP1CC, GIT2). The second ensemble was built over the aminoacyl-tRNA synthetase complex (AIMP1, AIMP2, KARS, RARS) and actin-binding protein PTK9 (also known as TWF1). The third ensemble was a mix of DNA stability regulators (CDC47, also known as MCM7; CDC21, also known as MCM4; SSBP1), trafficking regulators (COPB, COPG1) and general signaling nodes (SIPA1L1 and PPP2R3A).

Comparison of the OS-sensitive protein networks revealed that a node could harbor different phosphorylation dynamics according to different OS dynamics, triggering different cellular responses. These data highlight the existence of correlations between dynamic changes at the network level and decision-making processes, such as the decision to form either lamellipodia or invadosomes (Fig. 5E). Intriguingly, induction of lamellipodia correlated with increased phosphorylation amplitude of key regulators of this structure (p130CAS, ASAP2 and PP2AA) and late or sustained increased phosphorylation of EPHB2 and p120CAS. In contrast, invadosome formation correlated with decreased phosphorylation amplitude of key signaling relays (ASAP2, p130CAS), decreased enrichment of several acto-adhesive regulators (EPHB2, p120CAS) and sustained enrichment of key invasion regulators (PXN, SGK269, PTK9) and signaling regulators (PPP2R3A).

Instead of inducing binary phosphorylation, we determined that the modulation of OS dynamics was complex and characterized by its ability to diversely impact the temporal phosphorylation behavior of OS-sensitive signaling nodes. As our strategy to

Journal of Cell Science (2021) 134, jcs254599. doi:10.1242/jcs.254599

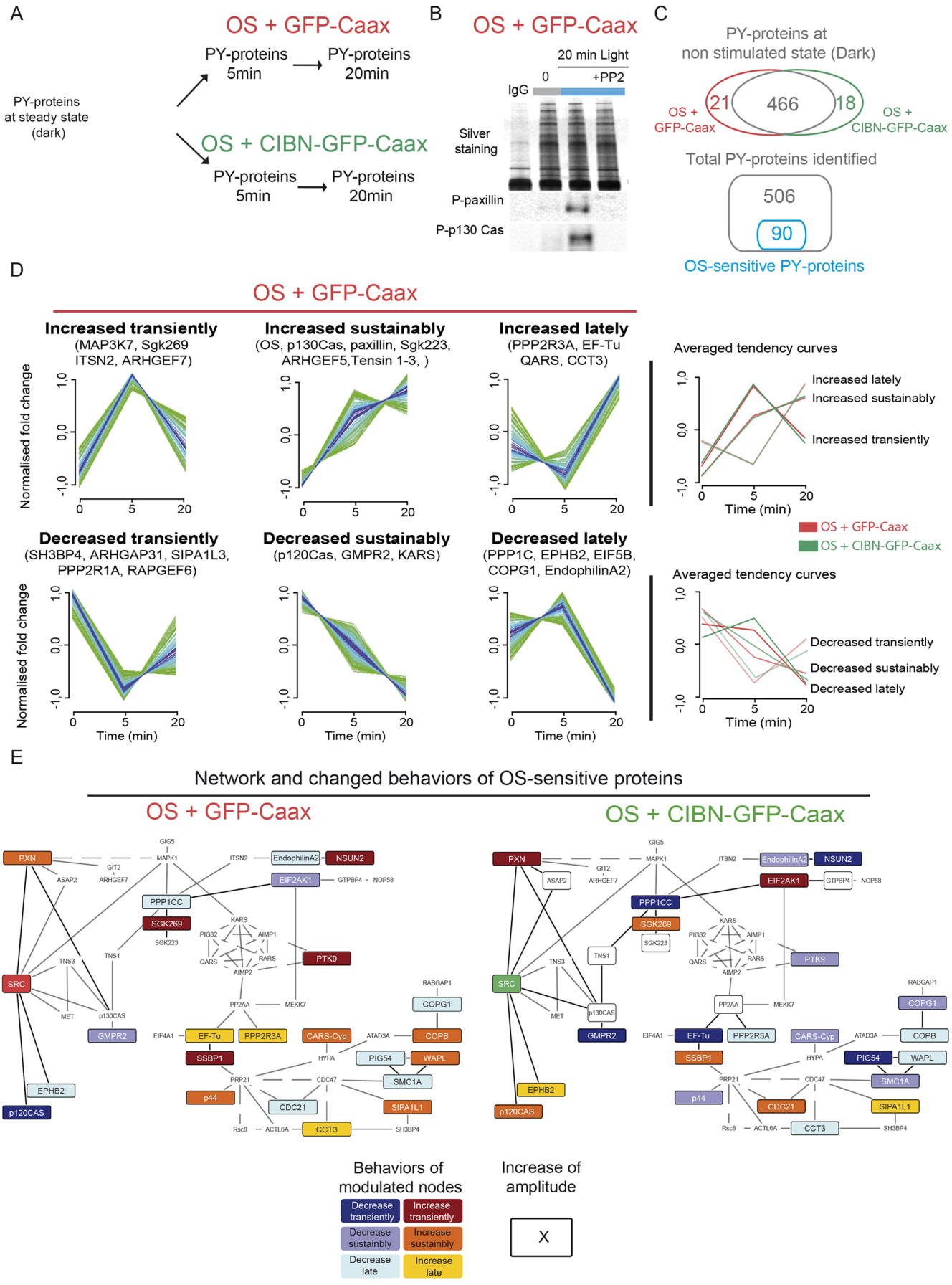

Fig. 5. See next page for legend.

Journal of Cell Science

Journal of Cell Science (2021) 134, jcs254599. doi:10.1242/jcs.254599

Fig. 5. Modulation of OS molecular flux in adhesive sites regulates different downstream signaling pathways. (A) Signaling pathways downstream of each OS flux were identified using time-resolved PY immunoprecipitation from photostimulated MDCK cells (blue light 50 ms pulse every min over 5 or 20 min). (B) Specific PY-enriched proteins were immunoprecipitated (silver staining) and showed that OS activation induces PP2-sensitive phosphorylation of classical c-SRC substrates such as p130CAS and paxillin. (C) Top: Venn diagram of identified PY proteins showing the high similarity between the OS+GFP–Caax (red) and OS+CIBN–GFP–Caax (green) conditions in the non-stimulated state. Bottom: OS-sensitive proteins represented only 17% of all PY proteins identified at time 0. (D) Detailed fuzzy c-means clustering analysis of OS-sensitive proteins observed in MDCK cells expressing OS+GFP–Caax. The dynamic behavior for each OS-sensitive protein is shown in green, grouped inside a cluster defined by the average trend (blue). Names of example OS-sensitive proteins are given for each cluster. Comparing averaged tendency curves showed high similarity for each cluster between each OS flux conditions. (E) Potential physical connections between OS-sensitive proteins were revealed by direct protein–protein interaction networks. OS-sensitive proteins (or nodes) presenting only a change in the amplitude of phosphorylation between conditions are outlined, and any OS-sensitive proteins presenting a change of phosphorylation behavior between conditions are color coded.

modulate the flux of OS oligomers at adhesive sites was based on large changes in the dimensionality of their mobility, we wondered whether a subtle modulation of OS dynamics was sufficiently sensitive to affect cellular responses.

Importance of the UD to modulate OS signaling flux

Previous structural studies support the existence of a role for the UD domain in the regulation of SH3-binding activity of SRC (Arbesú et al., 2017). Thus, we optogenetically investigated both the poorly known *in vivo* functions of this intrinsically disordered region (IDR) in SRC signaling (Arbesú et al., 2018) and the possibility of slightly modulating the flux of OS oligomers to adhesive sites by changing the binding properties of the SH3 domains without changing the dimensionality of OS mobility. Deletion of the UD in OS (OSΔUD) led to a significant increase in recruitment to adhesive sites compared with that of OS in response to TIRF photostimulation (33 mHz; Fig. 6A,B), suggesting that the UD behaved as a negative regulator of SH3-domain binding to PRR proteins in adhesive sites. Deletion of the UD did not affect the residence time of OS in adhesive sites (Fig. S6C). Therefore, OSΔUD was used to test the importance of modulating only signaling density and OS concentration in adhesive sites. Phenotypically, UD deletion slightly affected OS oligomer flux to adhesive sites, and this was sufficient to increase the percentage of cells forming invadosomes twofold in comparison to cells expressing full-length OS (Fig. 6C,D).

To determine the importance of this subtle change of OS flux of downstream signaling pathways, we analyzed the network architectures and dynamics of OS-sensitive proteins from photostimulated MDCK cells stably expressing OS or OSΔUD. Scaling up materials and improving the enrichment allowed us to identify more OS-sensitive proteins for each time point, consequently improving the depth of analysis (Table S2). We found that only a quarter of PY proteins identified at time 0 were directly modulated by OS photostimulation (255 OS-sensitive proteins out of 894 PY proteins; Fig. S6D) and had again a high probability of being SRC substrates (Table S2). Numerous proteins or GO functions identified after activation of MDCK cells stably expressing OS+GFP–Caax were also found after activation of cells stably expressing OS (Fig. S6E). Fuzzy c-means partitioning analysis organized these proteins into six clusters of temporal enrichment behaviors (Fig. S6F, Table S2).

To reduce the complexity of the networks downstream of both OS fluxes, we focused on the OS-sensitive proteins implicated in acto-adhesive regulation (63 out of 255; Fig. 6E). A large number of these proteins were previously identified (Fig. 5) and found to be physically connected. Comparison of the networks of OS-sensitive proteins demonstrated that most acto-adhesive proteins were not affected by the slight change of OS flux induced by UD deletion. However, consistent with a stronger recruitment of OSΔUD to adhesive sites, important invadosome regulators (PTPN6, ARAP3 and ARHGEF5) presented an increased amplitude of enrichment. On the other hand, a subtler response was obtained for other nodes, which either showed decreased phosphorylation (e.g. paxillin) or changes in their phosphorylation behavior, such as components of the COP9 signalosome, regulators of membrane trafficking (RAB11FIP1 and SEC16L, also known as SEC16A), thereby suggesting their involvement in invasion control. Finally, we observed that activation of OSΔUD also stimulated a functional complex composed of the GTPase CDC42, its guanine nucleotide-exchange factor (GEF) FGD6 and its effector tyrosine kinase ACK1 (also known as TNK2).

In addition to precisely characterizing the *in vivo* function of an IDR, the UD domain, the comparison of activated OS and OSΔUD dynamics in the same subcellular compartment identified a set of highly sensitive signaling nodes that are responsive to subtle modulation of OS flux over time.

DISCUSSION

To investigate the SRC coding activity, we engineered and specified uses of photoactivable SRC kinase to achieve spatio-temporal control of SRC in adhesive sites. We demonstrated that modulations of molecular fluxes of SRC activity were sufficient to hijack SRC pleiotropy, generating different downstream signaling pathways and ultimately triggering different cellular responses.

Engineering synthetic SRC in order to understand its complex structure–function relationship

Directly controlling SRC signaling in space and time is challenging. Previous protein engineering-based approaches have directly targeted the kinase domain of SRC by regulating its selectivity, folding or allostery (Chu et al., 2014; Garske et al., 2011; Karginov et al., 2010, 2014; Shah et al., 1997). Chemogenetic approaches are highly specific but are not suitable to achieve minute-scale and reversible control of this kinase at the subcellular level. Coupling allosteric regulation of SRC kinase and the light-sensitive domain Lov2 allowed generation of a photo-inhibitable SRC that is reversible and can present subcellular precision, but without activating specific and exogenous SRC signaling events (Dagliyan et al., 2016). In order to activate SRC in space and time, we engineered a photoactivable SRC based on a non-transforming v-Src mutant deleted of its membrane anchoring domain (Cross et al., 1984). In addition to improving the spatial resolution of the CRY2-based system (Valon et al., 2015), engineering OS also allowed control of the activation/deactivation cycle of SRC with high temporal range (minute scale) and revealed new functions of SRC oligomers and the UD, a simple IDR sufficient to regulate phenotypic specificity of SFKs (Summy et al., 2003). Despite SRC being mostly described as a monomer, controlling oligomerization with light is physiologically relevant, because SRC and other SFKs have been shown to dimerize, oligomerize and form larger nanoclusters after activation, although the functional relevance of these organizations *in vivo* is not known (Irtegun et al., 2013; Rossy et al., 2012; Smith et al., 2016; Spassov et al., 2018). Thus, our synthetic OS strongly supports that SRC

Journal of Cell Science (2021) 134, jcs254599. doi:10.1242/jcs.254599

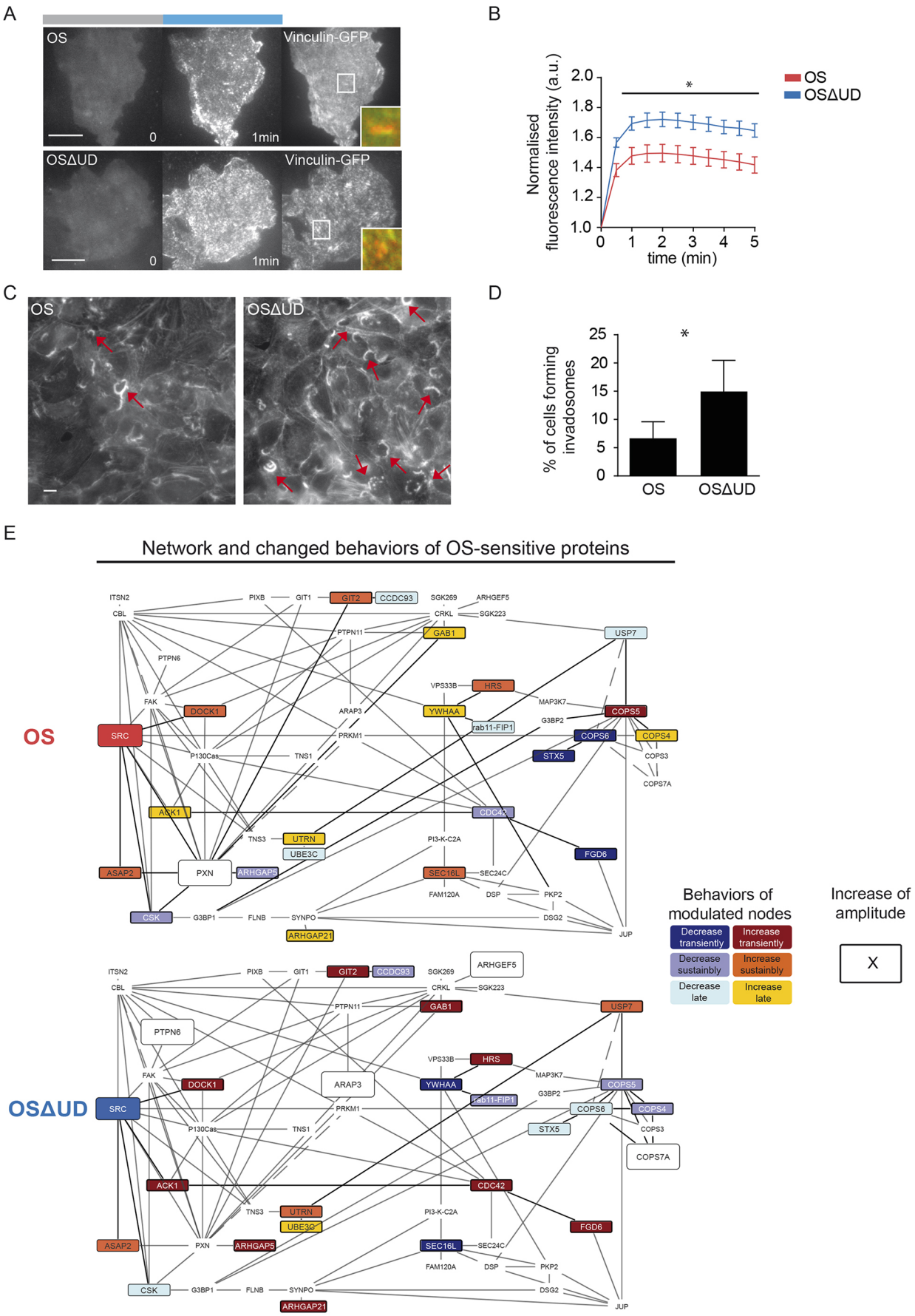

Fig. 6. See next page for legend.

Journal of Cell Science

Journal of Cell Science (2021) 134, jcs254599. doi:10.1242/jcs.254599

Fig. 6. Low modulation of OS oligomer flux in adhesive sites by deletion of the UD is sufficient to regulate cellular response and downstream signaling transfer. (A) Representative TIRF time series of OS and OSΔUD relocalization in adhesive sites (visualized using vinculin–GFP) after cyclic blue light TIRF photostimulation of MDCK cells (blue bar, 50 ms pulse every 30 s). White boxes indicate regions shown enlarged in inset images. (B) Quantification of OS and OSΔUD relocalization at the whole basal level of photostimulated MDCK cells (50 ms TIRF pulse every 30 s over 5 min). Data are presented as mean±s.e.m. N=3, >16 cells per condition. *P<0.05 (unpaired t-test). (C) Representative confocal images of invadosome rings (arrows; visualized using Alexa488–phalloidin) in OS and OSΔUD MDCK cells photostimulated for 15 min. (D) Quantification of the percentage of cells forming invadosomes in MDCK cells photostimulated for 15 min. Data are presented as mean±s.e.m. N=3, 300 cells per condition. *P<0.05 (paired t-test). (E) Connectivity between OS-sensitive proteins implicated in acto-adhesion and trafficking was revealed by direct protein–protein interaction networks. OS-sensitive proteins (or nodes) presenting only a change in the amplitude of phosphorylation between conditions are outlined, and any OS-sensitive proteins presenting a change of phosphorylation behavior between conditions are color coded. Scale bars: 5 µm.

oligomerization could be a new stabilizing process in adhesive sites mediated by SH3 domains and a late stage of activation. The apparent contradiction of essential roles for SH2 (Yeo et al., 2006) or SH3 (Fincham et al., 2002; Wu et al., 2016) domains in SRC relocalization to adhesive sites can now be explained if one assumes that the level of SRC oligomerization is involved, probably controlling specific partnerships with a large repertoire of PRR-containing proteins present in adhesive sites. Because a minimal level of multivalency of SH3 domains drives phase separation (Li et al., 2012), we hypothesized that OS oligomerization favors SH3 domain cooperativity that supports an increase in the apparent affinity of SH3 domains, leading to new binding when SRC molecules are grouped in nanoclusters. Moreover, only the use of OS allowed us to confirm the new and essential roles of the UD in the stabilization of SRC oligomers in adhesive sites, explaining its ability to modulate the SRC-substrate repertoire *in vivo*. In addition to modulating c-SRC adaptor functions, formation of oligomers also controls kinase activation. CRY2-mediated light-induced dimerization of cytosolic OS was sufficient to strongly increase Y416 phosphorylation (Fig. 3) and confirmed the existence of a transphosphorylation process (Vojtěchová et al., 2006).

By integrating intermediates of a signaling node and getting closer to its characteristic spatio-temporal activation patterns, the synthetic approach of optogenetics is complementary to long-term genetic manipulations for exploring new aspects of molecular dynamics *in vivo* in the decision-making activity of signaling nodes.

Biological relevance of synthetic OS

Our synthetic approach was based on deconstructing some regulatory elements of SRC, and this naturally raises the question of its biological relevance. The fact that SRC mutants containing SH2 or SH3 domain deletions can restore invadosome functions in *c-Src*$^{-/-}$ osteoclasts (Destaing et al., 2008) supported our assumption that other domains of SRC compensate for the loss of function of point-mutated SH2 domain. Moreover, we found that OS activation rapidly induced multiple physiological and classical c-SRC-dependent cellular structures, such as adhesive sites and actin cytoskeleton structures (Playford and Schaller, 2004). Indeed, OS activation induces dorsal ruffles, as seen previously for activation of a thermo-sensitive SRC mutant (Mettlen et al., 2006) and the activation of chemo-controllable synthetic SRC, containing both functional SH2 and SH3 domains (Gentry et al., 2016; Karginov et al., 2010). OS activation on membrane-induced lamellipodia in epithelial cells, suggesting activation is a partial epithelial–mesenchymal transition process that is in line with a previous report showing that only this mode of activation induced mechanical remodeling of epithelial layers (Moitrier et al., 2019). In MDCK cells, another mode of OS activation even induced invadosome rings, which are typical c-SRC-dependent structures in physiological and pathological conditions, as revealed by the study of *c-Src*$^{-/-}$ models (Boateng and Huttenlocher, 2012; Luxenburg et al., 2006). Preliminary results on photoactivated optoYes, another member of the SFK family poorly present in adhesive sites, revealed its inability to be recruited in adhesive sites in response to light (O.D., unpublished). This clearly confirmed the specificity of OS to be relocalized in adhesive sites and that our optogenetic approach cannot force SFK molecules to do something that they cannot achieve physiologically. Moreover, activation of optoSRC in SYF cells induced the activation of its kinase domain and the phosphorylation of paxillin in the same range as WT cSRC expressed in SYF cells, showing that its level of activation is in a physiological range comparable to that of WT c-SRC (Fig. S5B). In addition, activation of OS activated ERK pathways in the same range as physiological stimuli of SRC, such as EGF treatment or adhesion on extracellular matrix (ECM) (Fig. S2). Finally, mass spectrometry analysis clearly showed that known physiological substrates of SRC are phosphorylated in minutes in response to OS photostimulation (including the main SRC substrates paxillin, p130CAS, tensins, ASAP2, ARHGEFs and ephrins). It is important to note that most of these substrates are already known to be phosphorylated downstream of physiological stimulations such as PDGF and EGF treatments or adhesion on ECM.

In conclusion, it is striking to observe that our synthetic approach of SRC activation is sufficient to activate numerous and characteristic physiological features of c-SRC signaling pathways. Thus, this synthetic optogenetic probe provides a new direction to explore the causal link between SRC molecular dynamics *in vivo* and its associated signaling.

Control of OS molecular flux affects decision making in SRC signaling

Besides providing a simple qualitative activation approach and decreasing the repertoire of potential SRC conformational intermediates, we showed that specific cyclic and sustained optogenetic activation allowed us to control both duration and quantity of activated OS molecules relocalizing to adhesive sites over time. Thus, this relocalization-based strategy of our optogenetic design allowed us to integrate both quantity and duration of the transport of active OS molecules in an adhesive surface, which can be only described by the notion of flux of signaling OS molecules. The notion of flux of signaling has been proposed to explain the importance of changes to Cdc42 activation during cell polarization of budding yeast and has been used to model *in silico* enhanced activation or choice between alternative signaling pathways (Rapali et al., 2017; Selvarajoo et al., 2008). By only regulating either the local density of CRY2-dependent OS oligomers (by deletion of the UD) or the dimensionality of their mobility (by controlling membrane-based recruitment) over time, we could experimentally show that this is sufficient to induce different sustained fluxes of the same CRY2-dependent OS oligomers in adhesive sites. As a consequence, and independently of different frequencies of stimulation, our data showed that modulation of the flux of OS molecules in adhesive sites was sufficient to encode different decision-making events, leading to the formation of different acto-adhesive responses: invadosomes versus

Journal of Cell Science (2021) 134, jcs254599. doi:10.1242/jcs.254599

lamellipodia (Fig. 2E). Interestingly, we were not able to induce both invadosomes and lamellipodia at the same time, even though the two structures are not antagonistic. This rather suggests that the decision-making process induced here is exclusive. Finally, we showed high sensitivity of SRC decision-making events, because low amplitude modulation of OS molecular flux was sufficient to finely tune cell signaling to initiate specific pathways and acto-adhesive phenotypes (Fig. 6).

Beyond predicting that the probability of phosphorylation for any substrate is dependent on both local concentration of OS and OS residence time, we did not provide a strong model to explain how changing the flux of OS oligomers can support these decision-making processes. Since our approach revealed the importance of modulating the dynamics of the SRC molecule, it is important to remember that stochastic reactions occurring in biological processes between small number of molecules mean we must consider the inevitable randomness of their physical transport and binding reactions (Kaizu et al., 2014). In the specific case of the dynamics of OS oligomers relocalized to adhesive sites, it appears essential to consider the probability of OS oligomer rebinding to their substrates after a dissociation event: either OS oligomers bind a new substrate (after diffusing back into the bulk) or they rebind the same substrate. Considering both scenarios is essential to determine the probability of a kinase promoting mono-phosphorylation or multi-phosphorylation (on adjacent or distant sites) of the same protein. This physical principle of molecular dynamics has been used to show that MAPK and integrin signaling rely on the regulation of molecular mobility through cytosol-to-membrane relocalization or clustering of receptors (Block et al., 2015; Kholodenko et al., 2000). Thus, comparing flux of OS oligomers associated or not with membrane could represent two extreme cases where the flux of OS oligomers exchanging quickly with the cytosol could rather promote mono-phosphorylation or multi-phosphorylation on adjacent sites of a substrate. Thus, differences in flux of SRC could explain how this single kinase can control multiple possible phosphorylation sites of its main substrate, paxillin, in different conditions of activation or in different structures (lamellipodia versus invadosomes; Webb et al., 2005). Future coupled optogenetics and phosphopeptide studies will be necessary to determine how the coexistence of both fluxes of SRC and its potential substrates (Horton et al., 2016) at adhesive sites is integrated in order to affect the selection and multi-phosphorylation processes of specific signaling pathways. Thus, our optogenetics approach is an experimental proof-of-concept of a new direction to better understand the molecular basis for the activity of pleiotropic molecules in cell signaling.

Modulation of SRC molecular dynamics alters the phosphorylation dynamics of SRC substrates

To understand how subtle modulations of the OS flux coordinate different cellular responses, we mapped the downstream signaling pathways associated with each decision-making process. Although time-resolved phosphoproteomics has been used to globally determine the signaling events downstream of EGFR and TGF-β activation (D'Souza et al., 2014; Olsen et al., 2006), it has not previously been coupled to optogenetic studies to follow the dynamic emergence of a signaling pathway and its different associated cellular responses. In regard to the associated phenotype downstream of each OS flux, we generated biologically relevant data, because we identified key regulators of SRC-driven invadosome formation, such as paxillin and SGK269, and key regulators of lamellipodia, such as p130CAS, EPHB2 and p120CAS (Boguslavsky et al., 2007; Zhang et al., 2014; Zisch et al., 2000).

Our analysis tool revealed the existence of distinct classes of phosphorylation behavior (clusters) of OS-dependent substrates (Fig. 5D). Modulation of OS flux was sufficient to change the OS-substrate membership in each of these classes of phosphorylation behavior (Fig. 5E). This ability supports the decision-making switch associated with lamellipodia or invadosome formation, such as for EPHB2 or p120CAS (Fig. 5E). Modest modulation of OS oligomer fluxes (OS versus OSΔUD experiments) could affect the functional coupling between acto-adhesive and ECM degradation activities of invadosomes, which is supported by trafficking of WASH-associated endosomes (Monteiro et al., 2013). Indeed, this could occur through the regulation of the CDC42–FGD6–ACK1 complex, which is in agreement with the involvement of activated CDC42 in all invadosome models (Di Martino et al., 2014), the role of its GEF, FGD6, in the regulation of WASH-positive endosome trafficking (Steenblock et al., 2014) and the phosphorylation of the invadosome marker cortactin by ACK1 (Kelley and Weed, 2012).

Signaling networks are usually categorized in systems biology according to their sensitivity, redundancy and decision-making properties (Azeloglu and Iyengar, 2015). We believe that for SRC signaling in our experiments, these properties are, at least in part, under the direct control of OS flux. Indeed, modulation of c-SRC flux is sensitive enough to induce different phosphorylation dynamics of different members of the same family (SGK269 and SGK223, tensin-1 and tensin-3, GIT1 and GIT2) and generates redundancy represented by all OS-sensitive proteins without phosphorylation behavior changes.

Exploration of the OS activation regimen revealed new insights into the causal link between molecular signaling and decision making. This approach paves the way to understand the molecular basis of the pleiotropic coding of other signaling nodes and how oncogenic SRC signaling leads to physio-pathological transitions.

MATERIALS AND METHODS

Details of key resources used in this study are provided in Table S3. Additional details of recombinant DNA constructs are reported in Table S4.

Experimental cell models and culture

Experiments were performed on fibroblasts, SYF cells or epithelial MDCK cells transiently transfected and/or stably transduced using a viral strategy. All cell lines were cultivated at 37°C and 5% CO2 in DMEM high glucose (4.5 g/l) plus glutamax (PAA Laboratories) medium supplemented with 10% fetal bovine serum (GE Healthcare) and penicillin and streptomycin 1% (v/v) (PAA). All cells were transfected using Lipofectamine2000 according to the manufacturer's protocol (Invitrogen).

OptoSRC plasmid construction

In this study, c-SRC refers to the wild-type endogenous protein, whereas SRC refers to c-SRC-like activity induced by c-SRC mutants. The various OS plasmids are the result of C-terminal fusion of CRY2–mCherry to the indicated SRC mutants. All expression plasmids are listed in Table S4. All the OS and mutant plasmids were constructed from an Nhe1- and Not1-digested pSico backbone and sequences amplified by PHUSION high fidelity DNA polymerase (NEB) using Gibson assembly (NEB) following the supplier's instructions.

Lentivirus production, cell infection and sorting

Lentiviruses were produced by co-transfecting pC57GPBEB GagPol MLV, pSUSVSVG (gifts of Dr Nègre, ANIRA Platform, SFR Biosciences, Lyon, France) and each plasmid of interest using Lipofectamine2000 (Invitrogen) in HEK293 FT cells (gift of Dr Nègre) plated in 6-well plates at 50% confluency. The medium was changed 24 h later. The viral supernatant was collected after 72 h and was filtered with 0.45 µm filters. MDCK cells were plated in 6-well plates so as to achieve 60% confluency on the day of

infection. The filtered supernatant was directly used to infect cells of interest. The medium was changed 24 h after infection. After 10 days decontamination, cells were FACS sorted (Aria cell sorter 2000, BD) based on the level of expression of mCherry-tagged OS, using excitation with a 561 nm LASER.

Optogenetics experiments based on live-cell imaging, FRAP and large cell population activation

Live imaging, photostimulation and FRAP were performed with an iMIC inverted microscope (FEI) using time-lapse transmission, confocal (spinning disk) and TIRF imaging (63×/1.46 oil Korr M27; camera EMCCD, image acquisition with the LA software). Optogenetic activation of cells was classically achieved by cyclically stimulated them with one 488 nm TIRF excitation (50 ms) every 30 s over few minutes (33 mHz). OS basal membrane and adhesion site recruitment was followed using 561 nm TIRF imaging, while vinculin–iRFP or LifeAct–iRFP were monitored with 640 nm TIRF imaging. FRAP analysis was performed on an MDCK cell line stably expressing OS with or without CIBN–GFP–Caax and OS ΔUD using an iMIC inverted microscope (FEI) and the same 488 nm TIRF protocol (33 mHz) to photostimulate OS during the 4 min before the FRAP experiment. Laser photobleaching of activated OS in adhesive sites were performed with a 561 nm laser (100%) for 150 ms (with a bleach area of 10×10 µm). Recovery of activated OS in adhesive sites was recorded every 400 ms for 1 min. FRAP analyses were performed using OA offline analysis software with the offline FRAP tool/option (FEI). After normalization on the total cell intensity and on the camera background, a single exponential model was applied: $A\times(1-e^{-t\times\tau^{FRAP}})$, in order to measure both characteristic time of recovery and the immobile fraction.

Besides single-cell analysis, large cell population photostimulation was performed using a homemade blue LED plate (constructed by C. Tucker, I. Wang and M. Balland, Lihpy, Grenoble-Alpes University). The LED illuminations were programmed using Arduino software at 2 min frequency (8.33 mHZ, 200 ms single exposure) at 50% LED power for 5 or 20 min.

PY immunoprecipitation and proteome identification

To characterize the protein–protein interaction networks supporting OS-sensitive signaling pathways, we purposely used PY co-immunoprecipitation rather than phosphopeptide purification to identify both OS substrates and their regulators. Large cell populations were photostimulated using a homemade blue LED plate before lysis and PY-associated protein purification. Six million MDCK cells stably expressing OS in different conditions (OS with or without CIBN–GFP–Caax, and OS with or without the ΔUD mutation) were plated and allowed to adhere for 24 h. Cells were starved for 12 h in DMEM medium before photostimulation. For some control conditions, inhibition of any SFK activity was achieved by treating MDCK cells with 10 µM PP2 (Calbiochem, 529576) 30 min before photostimulation. Cells were harvested in modified RIPA lysis buffer [150 mM NaCl, 20 mM Tris-HCl (pH 7.4), 1% NP40, 0.5% sodium deoxycholate, 0.1% SDS, 1× cOmplete EDTA-free protease inhibitor cocktail (Sigma #11836170001) and an antiphosphatase mix of 1 mM orthovanadate, 10 mM sodium fluoride and 10 mM glycerophosphate]. Proteins (1.5 mg) in lysates were pre-cleared with Protein G Sepharose beads (Fast flow; Sigma, #P3296), then PY were immunoprecipitated using 5 µg of antibodies (PY1000, Cell Signaling Technology, #8954 and 4G10, Millipore, #05-321) or IgG2B for the IgG control (BD Biosciences, BD557351) at 4°C for 4 h in a rotation wheel. 50 µl of Protein G Sepharose was then added for 1 h before being washed three times. The pellet was centrifuged at 2000 ***g*** for 2 min at 4°C before resuspension in 50 µl of 3× Laemmli buffer.

Mass spectrometry-based proteomic analyses

Three replicates per condition were analyzed. Immunoprecipitated eluates were solubilized in Laemmli buffer, separated by SDS-PAGE (4–12% NuPAGE gel, Invitrogen) and stained using R-250 Coomassie Blue (BioRad). After elimination of bands corresponding to heavy and light chains of IgG, the whole content was in-gel digested using trypsin (Promega), as previously described (Casabona et al., 2013). Resulting peptides were analysed by nanoliquid chromatography coupled to tandem mass spectrometry (Ultimate 3000 coupled to LTQ-Orbitrap Velos Pro, Thermo Scientific) using a 120 min gradient. RAW files were processed using MaxQuant version 1.5.8.3. Spectra were searched against the Uniprot database (*Canis lupus familiaris* taxonomy, April 2017 version), the sequence of OS and the frequently observed contaminants database embedded in MaxQuant. Trypsin was chosen as the enzyme and two missed cleavages were allowed. Precursor mass error tolerances were set at 20 ppm and 4.5 ppm for first and main searches, respectively. Fragment mass error tolerance was set to 0.5 Da. Peptide modifications allowed during the search were carbamidomethylation (C, fixed), acetyl (protein N-ter, variable) and oxidation (M, variable). Minimum peptide length was set to seven amino acids. Minimum number of peptides, razor+unique peptides and unique peptides were all set to 1. Maximum false discovery rates – calculated by employing a reverse database strategy – were set to 0.01 at peptide and protein levels. Protein intensities were calculated from extracted mass spectrum intensities of razor+unique peptides and used for statistical analyses with ProStaR (Wieczorek et al., 2017). Proteins identified in the reverse and contaminant databases and only identified by site were discarded. After $\log_2$ transformation, intensity values were condition-wise median normalized, missing data imputation was realized (replacing missing values with the first-percentile value of each column) and statistical testing was conducted using a limma *t*-test. Proteins were considered as differentially expressed between immunoprecipitations performed using control IgG and PY IgG if they exhibited a $\log_2$ fold change greater than 1 or less than −1 and a *P*-value inferior to the cut-off fixed to reach a false discovery rate (FDR) of less than 1%, calculated using the Benjamini–Hochberg method. The list of proteins to be considered for the timecourse analyses was built by aggregating the proteins found to be differentially expressed between immunoprecipitations performed using control IgG and PY IgG at 0 min, 5 min and 20 min. Raw intensities were median normalized and missing value imputation was performed condition by condition using the first-percentile value of each column if no value was present or by the k-nearest neighbor (k-NN) method if at least one value was present. Statistical testing was then conducted using a limma *t*-test.

Post-analysis of protein lists generated by mass spectrometry and time-resolved analysis pipe-line

Analysis of variation in temporal enrichment of proteins in datasets

Missing protein identifiers from *Canis lupus familiaris* were manually mapped to *Homo sapiens* after blast analysis (www.uniprot.org/blast/), applying >85% threshold of homology for successful identification. R environment (R Development core team, 2008) was used together with fuzzy c-means analysis to define clusters of temporal variation in the mean intensity of proteins that had a statistically significant difference in intensity between 5 or 20 and 0 min samples (Kumar and Futschik, 2007), both separately and for each dataset (OS+GFP–Caax or OS+CIBN–GFP–Caax; OS or OSΔUD). We iteratively explored combinations of cluster sizes and fuzzification parameters to find optimal partitioning parameters to compare the OS+GFP–Caax and OS+CIBN–GFP–Caax data sets (c=6, m=3).

Average trends were plotted to define cluster correspondence, with default behavior set on OS+GFP–Caax for OS+GFP–Caax versus OS+CIBN–GFP–Caax comparison, or to OS for OS versus OSΔUD comparison. Significance of variation between datasets was further supported by limma *t*-test at 5 and 20 min between OS+GFP–Caax/OS+CIBN–GFP–Caax or OS/OSΔUD. When soft clustering and limma *t*-test were in agreement, we concluded for a cluster change or a lack of change in temporal trend according to fuzzy c-mean results. In contrast, in the case of disagreement between soft clustering and limma *t*-test, we analyzed the temporal trends one-by-one using a homemade R script to conclude whether or not the cluster had a change in temporal trend. If a difference was confirmed by limma *t*-test but did not present any cluster change, we concluded that these proteins present the same behavior but are associated with a significant change of the amplitude of this behavior (indicated as 'increase of amplitude' in Fig. 5E and Fig. 6E). In addition, out of 24 proteins in this case in OS+GFP–Caax versus OS+CIBN–GFP–Caax analysis, we eventually validated a temporal trend change for CCT3, EEF1A1, MED13, PPP1CC and PPP2R3A. Likewise, out of 124 proteins in the OS versus OSΔUD analysis, we validated a temporal trend change for MTA1, NACA, NOP56, SAR1B, SLC25A3, SRPK1, SUCLA2 and

ZWILCH. In both analyses, the majority of the remaining proteins from this population were considered as temporally unaltered by OS modulation. To assess and compensate for potential proteome variations that might arise during cell strain establishment, we systematically compared temporal trends of proteins differentially enriched at 0 min. All proteins enriched at 0 min were removed from further analysis if the temporal trends in compared datasets were identical to each other.

As such, CDCP1 and TACC1 were removed from OS+GFP–Caax versus OS+CIBN–GFP–Caax network analysis, whereas PTPN23, ARHGEF5, PTPN6, SEC16A, EIF3E, CLASP2, HSD17B4, COPS7A, TMRT6, N4BP2, CPSF7, ANKRD17, OSBPL3 and ARAP3 were removed from OS versus OSΔUD network analysis. SRC interaction likelihood, protein–protein interaction network reconstruction and Gene Ontology enrichment analysis were performed on the resulting 0 min-subtracted protein lists.

Assessment of SRC substrate likelihood

To determine the biological relevance of identified proteins, we looked for interaction with SRC in the BIOGRID database (Chatr-Aryamontri et al., 2017; database gathered on 28 November 2017 via PSICQUIC services). In addition, we crossed our results with a list of human proteins annotated with phospho-tyrosine among the reviewed proteins in the Uniprot database. We also assessed the potentiality of targeting candidates according to the GPS tool (Xue et al., 2011). In this case, FASTA sequences of proteins were retrieved from the Uniprot database, and the consensus sequence for phosphorylation by SRC was searched by conservatively setting the results threshold to high filter (and score >1.5; reported as 'all' in Tables S1 and S2). To further increase the stringency of the prediction, we scored proteins that show either one or two sites with a score in the top first decile (high filter and score >10). Finally, a list of proteins sensitive to the SRC inhibitor PP2 at 20 min after OS activation was determined by limma *t*-test.

Gene Ontology enrichment

Lists of identified proteins were analyzed for enrichment of the three classes of ontologies: biological processes (BP), molecular functions (MF) and cellular components (CC), using the PANTHER overrepresentation test (http://amigo.geneontology.org/amigo; released on 13 April 2017) and GO ontology database release of 28 November 2017, with Bonferroni correction applied.

Protein–protein interaction network reconstruction and analysis

We reconstructed the protein–protein interaction network by gathering BIOGRID, INTACT and MINT protein-protein interaction data from *Homo sapiens* with PSICQUIC retrieval (gathered on 7 December 2017) and using the Cytoscape environment (Shannon et al., 2003). A custom-made approach was used to combine data from these bases, and edges information was implemented accordingly. We applied the discrimination procedure described above in the analysis of temporal enrichment, for proteins enriched at 0 min. In the case of OS+GFP–Caax versus OS+CIBN–GFP–Caax comparison, we defined the simplest model network representing all proteins that have either fuzzy c-mean cluster change and/or a temporal inter-dataset *P*-value. As mass spectrometry analysis identified more proteins in the OS versus OSΔUD comparison, we chose to describe only proteins with both a cluster change and a temporal interdataset *P*-value. We used the cluster identifiers with respect to temporal trend changes in layout to underline the differences described among datasets. When applicable, proteins without cluster change or inter-dataset temporal *P*-value were not color-coded and size-reduced on the graphic representations of the network. Upon request, generated network maps can be uploaded for public access on CyNetShare (http://cynetshare.ucsd.edu/).

Quantification and statistical analysis

Data were judged to be significant when $P<0.05$ by unpaired, two-tailed Mann–Whitney test. We denote statistical significance as follows: ns, not significant (i.e. $P>0.05$); *$P<0.05$; **$P<0.01$; ***$P<0.001$; ****$P<0.0001$. Graphs and statistical analyses were generated using Prism 6 (Graphpad), and the boxplots indicate the data distribution of the second and third quartile (box), median (line), mean (filled squares), and 1.53× interquartile range (whiskers).

Brightness analysis of OS oligomeric state

Fluorescence correlation spectroscopy (FCS) data acquisition was performed using a LSM710-Confocor3 confocal microscope (Carl Zeiss). The inverted AxioObserver stand was equipped with a C-Apochromat 40×/1.2 water-immersion objective, and the on-stage cell incubator (PeCon) and the overall environmental chamber were stabilized at 37°C at least 1 h before acquisitions. Cells were transfected and plated on 4-well chambered coverslips (LabTek) 24 h prior to the experiments at 37°C in 5% CO_2, and were maintained in those conditions throughout acquisition. The mCherry fluorescence was excited with a 561 nm DPSS laser, reflected by a 488/561 double primary dichroic filter. The laser light power of 2.6 µW was measured at the objective output at 0.3% AOTF transmission. The fluorescence was selected using a 580 nm long-pass secondary dichroic filter, and its fluctuations were sampled by the APD detector at 20 MHz rate. The laser power, pinhole alignment and the detected molecular brightness and mobility were carefully controlled on a day-to-day basis using a calibration solution of 15 nM sulforhodamine B (Sigma) in water. The shape parameter (axial-to-lateral size ratio) of the confocal volume of 6.9 was determined by fitting the calibration ACF curve to a single-component free diffusion model, and was fixed to this value in the following analyses. In cases of photostimulation of the optogenetic tag CRY2, the 488 nm line of the Ar laser (1% AOTF transmission) was activated simultaneously with a 561 nm FCS laser during acquisition. Due to the high mobility of the cytoplasmic pool of proteins, a stationary regimen of photoactivation was then established and maintained during FCS measurements after a short transition period of ∼30 s. Single FCS acquisitions were limited to 10 s and repeated ten times in a cytosolic region of the cell. The presence of the second 488 nm laser increased the apparent brightness of mCherry by ∼8% due to additional excitation in the absorption tail of the fluorophore spectrum. Moreover, the AOTF acousto-optic crosstalk was found to slightly modify the transmitted intensity of the 561 nm laser in the presence of 488 nm illumination. The obtained brightness values were accordingly corrected for the proper comparison between no-stimulation and stimulation conditions. The molecular brightness estimated from the FCS curve is also biased by fluorophore photobleaching and the cytosolic depletion during 488 nm photoactivation. In order to minimize these biases and to be less dependent on the fit quality of the FCS model, we estimated the molecular brightness from the raw photon counts over short time intervals according to the formula:

$$B = \left[\frac{\sigma^2}{\langle k\rangle - 1}\right]\frac{1}{\Delta t},$$

where $\langle k\rangle$ is the mean number of counts per bin time Δt, and σ^2 is the variance of photon counts. The bin time was chosen to be 150 µs because it is long enough in order to average out photoblinking effects and to obtain higher values of counts per molecule (CPM), but is still considerably shorter than the average diffusion time of the studied molecules, in order to validate the 'pseudo static' approximation. The 1 s integration intervals produce sufficient photon statistics for a good signal-to-noise ratio and are short enough to reduce the effects of photobleaching, cytosolic depletion and cell movements. The binary raw data were saved during the standard FCS acquisitions and were then rebinned and analyzed using a custom ImageJ macro. The molecular brightness within each cell was averaged from 60 points (the first 40 points are excluded due to the equilibrated state of the beginning of the photostimulation). Each average brightness was then averaged for the ∼15 cells studied in each condition.

Mathematical modeling of different OS fluxes

In order to specify the flux of OS recruitment following light activation, we consider the passive transport mechanisms of activated OS (OS dimers) in the cell volume either with adsorption on the cell membrane or on discrete adhesive sites (Fig. 4G). From the mathematical point of view, the model is valid in two or three spatial dimensions, but it is more tractable in 2D from the numerical point of view. The principal result reported from this modeling is illustrated in Fig. 4H, where it is demonstrated that the OS flux is sustained at a higher level and for a longer time when activated OS is directly recruited to adhesive sites without intermediate membrane

Journal of Cell Science (2021) 134, jcs254599. doi:10.1242/jcs.254599

adsorption. Explicit solutions for this problem are given to characterize the different time scales.

Call Ω the volume of a spherical cell of radius R_0 in arbitrary dimensions with boundary $\partial\Omega$. $\partial\Omega$ is either a circle in 2D or a sphere in 3D with the same radius. To compute the flux φ of activated OS per unit length or surface, consider an initial concentration $u_0(r)$ of light-activated OS in the bulk, where r is the radial vector distance to the origin. The model takes into account the diffusion of OS in the bulk with diffusion coefficient D and introduces an effective adsorption rate $k_a^*(r)$ on the boundary $\partial\Omega$. This rate of adsorption is proportional to the density $n_m(r)$ of adsorption sites on $\partial\Omega$. In the presence of CIBN–GFP–Caax, $n_m(r)$ is homogeneously distributed on the membrane and k_a^* is constant. In contrast, $n_m(r)$ is exclusively concentrated on the adhesive sites in the GFP–Caax case (see Fig 1 and Fig. 4H), and $k_a^*(r)$ varies on the boundary $\partial\Omega$:

$$k_a^*(r) = k_a n_m(r) \quad r \in \partial\Omega, \tag{1}$$

where k_a is the rate per unit surface at full coverage. To compare case one, where activated OS is recruited to the membrane, to case two, where OS is only recruited to clusters, we assume that $n_m(\theta)$ has a square wave distribution, with $n_m(\theta)$ alternating between 0 and n_m along the boundary. Following illumination, the two geometries give different flux densities. For the same buffer of cytosolic activated proteins, the flux through adhesive clusters in case two must be larger than in case one, since the same amount of material must be adsorbed at infinite time, but on a smaller spatial domain. Using this sink analogy, we also see that full adsorption takes a longer time on clusters than on a homogenous boundary.

To summarize, the concentration $u(r, t)$ solves the following problem:

$$\begin{aligned} \frac{1}{D}\frac{\partial u}{\partial t} &= \Delta u \qquad && r \in \Omega \\ u(r, t=0) &= u_0(r) && r \in \Omega \\ -D\hat{u}_r \nabla u(r,t) &= k_a^*(r) u(r,t) && r \in \partial\Omega, \end{aligned} \tag{2}$$

where the first two equations are the diffusion equation together with the initial condition at zero time. The last equation equals the flux φ of adsorption normal to the boundary with the probability that the protein is absorbed on a site assuming that they are in contact (Robin boundary condition). We are interested in computing the time dependent solution of Eqn 2 from which the total amount of OS can be calculated.

For what follows, it is useful first to consider the dimensionless ratio to compare the diffusion-limited rate of Schmoluchowski with the rate of OS association with the membrane assuming close contact,

$$\frac{k_a^* R_0}{D} \tag{3}$$

When this ratio is smaller than 1, we are in the fast diffusion regime where, following illumination, the concentration in the bulk first becomes homogenous, and OS proteins are subsequently adsorbed. This is the relevant experimental regime that ensures that our results will not depend on the geometry. Following initial bulk homogenization, the buffer of cytosolic proteins is cleared on a much longer time scale. Calculations below show that this occurs on a characteristic time scale t_1, which we compare with the diffusion time scale t_0:

$$t_1 = \frac{R_0}{2k_a^*} \quad t_0 = \frac{R_0^2}{4D}, \tag{4}$$

so that the flux φ exhibits a sharp increase at short times, $t<t_0$, and decreases more slowly at longer times, $t \simeq t_1$ (see Fig. 2). For a typical cytosolic protein with R_0=10 µm and D=10 µm^2 s^{-1}, t_0=2.5 s. Since typical association rates of proteins are of the order of 30 µM s^{-1}, t_1 is of the order of a few tens of seconds. In Eqn 2, we have neglected desorption. This approximation is valid if the characteristic time for this process is longer than all other characteristic times, and it has the advantage of decoupling the adsorption problem from the diffusion problem of adsorbed proteins along the boundary. If diffusion along the boundary occurs, desorption will take place homogeneously along the boundary with small modifications of the bulk diffusion flux contour lines, so that the problem is a good approximation at short time.

In the homogenous case one (indirect relocalization of activated OS in discrete adhesive sites through a membrane step as in the condition of expression of CIBN–GFP–Caax), our problem is solved in 2D by separation of variables $u(r,t) = \exp[-D\lambda_m^2 t]u(r)$. Sturm–Liouville theory gives the solution as a series:

$$u(r,t) = \sum_{m\geq 1} C_m J_0(\beta_m r) e^{-D\beta_m^2 t}. \tag{5}$$

The boundary condition in Eqn 2 gives the set $\{\beta\}_{m\geq 1}$ as the ordered set of positive roots of the equation:

$$\beta_m R_0 J_1(\beta_m R_0) = \frac{k_a^* R_0}{D} J_0(\beta_m R_0), \tag{6}$$

where $J_{0,1}(r)$ are standard Bessel functions. The coefficients c_m are obtained by operating on the initial condition:

$$c_m = \frac{1}{N(\beta_m)^2} \int_0^{R_0} dr\, r J_0(\beta_m r) u_0(r), \tag{7}$$

with

$$N(\beta_m)^2 = \int_0^{R_0} dr\, r J_0(\beta_m r)^2. \tag{8}$$

The limit of small $k_a^* R_0/D$ is interesting. In this limit,

$$\beta_1 R_0 \simeq \left[\frac{2k_a^* R_0}{D}\right]^{1/2} \ll 1. \tag{9}$$

Thus, according to Eqn 5, the characteristic time scale for the exponential decrease in flux density is:

$$D\beta_1^2 \simeq 2k_a^*/R_0. \tag{10}$$

We conclude that the first term in the series dominates and that the flux of proteins adsorbed on the membrane will decrease with a characteristic time $t_1 = R_0/2k_a^*$ after a sudden increase on time scale t_0. The same result holds for the 3D solution with the same symmetry of revolution. Eqn 5 should be adapted using the appropriate basis. Because of dimensional analysis, the same characteristic time scale enters into the problem.

In the non-homogenous case two (direct relocalization of activated OS in discrete adhesive sites as in the condition of expression of GFP–Caax), we solve Eqn2 using finite element methods for a square-wave distribution of clusters. For convenience, we take the density of adsorption sites in the square as equal to the density of adsorption sites for the homogenous membrane.

Fig. 4H compares the solution for the homogenous problem with the one for the cluster geometry with averaged quantities per unit length. Since the clusters occupy only 50% of the total perimeter, the area under the curves are the same when conveniently renormalized, so that the total amount of proteins absorbed is the same at infinite time. The two curves exhibit the same sharp increase at short time t_0, which only depends on diffusion in the bulk but not on cluster geometry. Again, the mean adsorbed flux is higher in the non-homogenous geometry than in the homogenous case and decreases slowly, because all material has to be only adsorbed on the discrete adhesive sites and not inbetween. Depending on the cluster geometry, this happens on different time scales, as can be seen from Eqn 4, by renormalizing the adsorption rate k_a^* by the fraction of the area occupied by the adsorption sites.

Note added in proof

After completing this work, we were informed that Shaaya et al., 2020 have published material that relates closely to the topic of the present study.

Acknowledgements
We acknowledge the benevolence and talent of Dr S. Wickström for critical reading of the manuscript. We also thank Dr C. Gaggioli, Professor R. Baron, Dr M. Coppey, Dr E. Miroshnikova, Professor A. Delon, Dr I. Wang, Professor M. Digman and Professor E. Graton for experimental help, critical reading and exciting discussions. We thank the support of the discovery platform and informatics group at EDyP.

Competing interests
The authors declare no competing or financial interests.

Author contributions
Conceptualization: A. Kerjouan, E.F., I.B., B.F., O.D.; Methodology: A. Kerjouan, C.B., C.O., E.H.-B., A.G., M.B., I.B., Y.C., B.F., O.D.; Software: C.B., A.G., B.F.; Validation: C.O., E.H.-B., M.P., O.D.; Formal analysis: A. Kerjouan, C.O., E.H.-B., A.G., A. Kraut, M.P., B.F., O.D.; Investigation: A. Kerjouan, E.H.-B., A.G., A. Kraut, M.P., B.F., O.D.; Resources: C.O., O.D.; Data curation: C.B., A.G., A. Kraut, Y.C., O.D.; Writing - original draft: A. Kerjouan, E.F., O.D.; Writing - review & editing: C.B., E.F., I.B., Y.C., B.F., C.A.-R., O.D.; Visualization: Y.C., B.F.; Supervision: O.D.; Project administration: O.D.; Funding acquisition: O.D.

Funding
This work was funded by the Agence Nationale de la Recherche JCJC program (ANR-13-JSV2-0003-01), by the Ligue Contre le Cancer as 'Equipe labellisée Ligue 2014' (EL2014.LNCC/CAR) and by the Fondation pour la Recherche Médicale as 'Equipe labellisée FRM 2017' (DEQ20170336702). The PhD of A. Kerjouan was funded by the Ligue Contre le Cancer (GB/MA/VSP 11211) and the Fondation pour la Recherche Médicale (FDT20170437267). Proteomic experiments were partly supported by the Agence Nationale de la Recherche Proteomics French Infrastructure (ANR-10-INBS-08-01) and Labex GRAL (ANR-10-LABX-49-01).

Data availability
Mass spectrometry proteomics data have been deposited to the ProteomeXchange Consortium via the PRIDE (Vizcaíno et al., 2016) partner repository with the dataset identifier PXD008534.

Supplementary information
Supplementary information available online at
https://jcs.biologists.org/lookup/doi/10.1242/jcs.254599.supplemental

References

Arbesú, M., Maffei, M., Cordeiro, T. N., Teixeira, J. M. C., Pérez, Y., Bernadó, P., Roche, S. and Pons, M. (2017). The unique domain forms a fuzzy intramolecular complex in Src family kinases. *Structure* **25**, 630-640.e4. doi:10.1016/j.str.2017.02.011

Arbesú, M., Iruela, G., Fuentes, H., Teixeira, J. M. C. and Pons, M. (2018). Intramolecular fuzzy interactions involving intrinsically disordered domains. *Front. Mol. Biosci.* **5**, 39. doi:10.3389/fmolb.2018.00039

Azeloglu, E. U. and Iyengar, R. (2015). Signaling networks: Information flow, computation, and decision making. *Cold Spring Harb. Perspect. Biol.* **7**, a005934. doi:10.1101/cshperspect.a005934

Bernadó, P., Pérez, Y., Svergun, D. I. and Pons, M. (2008). Structural characterization of the active and inactive states of Src kinase in solution by small-angle X-ray scattering. *J. Mol. Biol.* **376**, 492-505. doi:10.1016/j.jmb.2007.11.066

Block, M. R., Destaing, O., Petropoulos, C., Planus, E., Albigès-Rizo, C. and Fourcade, B. (2015). Integrin-mediated adhesion as self-sustained waves of enzymatic activation. *Phys. Rev. E Stat. Nonlin. Soft Matter Phys.* **92**, 042704. doi:10.1103/PhysRevE.92.042704

Boateng, L. R. and Huttenlocher, A. (2012). Spatiotemporal regulation of Src and its substrates at invadosomes. *Eur. J. Cell Biol.* **91**, 878-888. doi:10.1016/j.ejcb.2012.06.003

Boguslavsky, S., Grosheva, I., Landau, E., Shtutman, M., Cohen, M., Arnold, K., Feinstein, E., Geiger, B. and Bershadsky, A. (2007). p120 catenin regulates lamellipodial dynamics and cell adhesion in cooperation with cortactin. *Proc. Natl. Acad. Sci. USA* **104**, 10882-10887. doi:10.1073/pnas.0702731104

Casabona, M. G., Vandenbrouck, Y., Attree, I. and Couté, Y. (2013). Proteomic characterization of Pseudomonas aeruginosa PAO1 inner membrane. *Proteomics* **13**, 2419-2423. doi:10.1002/pmic.201200565

Chatr-Aryamontri, A., Oughtred, R., Boucher, L., Rust, J., Chang, C., Kolas, N. K., O'Donnell, L., Oster, S., Theesfeld, C., Sellam, A. et al. (2017). The BioGRID interaction database: 2017 update. *Nucleic Acids Res.* **45**, D369. doi:10.1093/nar/gkw1102

Chu, P.-H., Tsygankov, D., Berginski, M. E., Dagliyan, O., Gomez, S. M., Elston, T. C., Karginov, A. V. and Hahn, K. M. (2014). Engineered kinase activation reveals unique morphodynamic phenotypes and associated trafficking for Src family isoforms. *Proc. Natl. Acad. Sci. USA* **111**, 12420-12425. doi:10.1073/pnas.1404487111

Cross, F. R., Garber, E. A., Pellman, D. and Hanafusa, H. (1984). A short sequence in the p60src N terminus is required for p60src myristylation and membrane association and for cell transformation. *Mol. Cell. Biol.* **4**, 1834-1842. doi:10.1128/MCB.4.9.1834

Dagliyan, O., Tarnawski, M., Chu, P.-H., Shirvanyants, D., Schlichting, I., Dokholyan, N. V. and Hahn, K. M. (2016). Engineering extrinsic disorder to control protein activity in living cells. *Science* **354**, 1441. doi:10.1126/science.aah3404

Destaing, O., Sanjay, A., Itzstein, C., Horne, W. C., Toomre, D., De Camilli, P. and Baron, R. (2008). The tyrosine kinase activity of c-Src regulates actin dynamics and organization of podosomes in osteoclasts. *Mol. Biol. Cell* **19**, 394-404. doi:10.1091/mbc.e07-03-0227

Digman, M. A., Dalal, R., Horwitz, A. F. and Gratton, E. (2008). Mapping the number of molecules and brightness in the laser scanning microscope. *Biophys. J.* **94**, 2320-2332. doi:10.1529/biophysj.107.114645

Di Martino, J., Paysan, L., Gest, C., Lagrée, V., Juin, A., Saltel, F. and Moreau, V. (2014). Cdc42 and Tks5: a minimal and universal molecular signature for functional invadosomes. *Cell Adhes. Migr.* **8**, 280-292. doi:10.4161/cam.28833

D'Souza, R. C. J., Knittle, A. M., Nagaraj, N., van Dinther, M., Choudhary, C., ten Dijke, P., Mann, M. and Sharma, K. (2014). Time-resolved dissection of early phosphoproteome and ensuing proteome changes in response to TGF-. *Sci. Signal.* **7**, rs5. doi:10.1126/scisignal.2004856

Duan, L., Hope, J., Ong, Q., Lou, H. Y., Kim, N., McCarthy, C., Acero, V., Lin, M. Z. and Cui, B. (2017). Understanding CRY2 interactions for optical control of intracellular signaling. *Nat. Commun.* **8**, 547. doi:10.1038/s41467-017-00648-8

Fincham, V. J., Brunton, V. G. and Frame, M. C. (2002). The SH3 domain directs acto-myosin-dependent targeting of v-Src to focal adhesions via phosphatidylinositol 3-Kinase. *Mol. Cell. Biol.* **20**, 6518-6536. doi:10.1128/MCB.20.17.6518-6536.2000

Garske, A. L., Peters, U., Cortesi, A. T., Perez, J. L. and Shokat, K. M. (2011). Chemical genetic strategy for targeting protein kinases based on covalent complementarity. *Proc. Natl. Acad. Sci. USA* **108**, 15046-15052. doi:10.1073/pnas.1111239108

Gentry, L. R., Karginov, A. V., Hahn, K. M. and Der, C. J. (2016). Characterization of an engineered Src kinase to study Src signaling and biology. *Methods Mol. Biol.* **1360**, 157-167. doi:10.1007/978-1-4939-3073-9_12

Horton, E. R., Humphries, J. D., Stutchbury, B., Jacquemet, G., Ballestrem, C., Barry, S. T. and Humphries, M. J. (2016). Modulation of FAK and Src adhesion signaling occurs independently of adhesion complex composition. *J. Cell Biol.* **212**, 349-364. doi:10.1083/jcb.201508080

Irtegun, S., Wood, R. J., Ormsby, A. R., Mulhern, T. D. and Hatters, D. M. (2013). Tyrosine 416 is phosphorylated in the closed, repressed conformation of c-Src. *PLoS One* **8**, e71035. doi:10.1371/journal.pone.0071035

Kaizu, K., de Ronde, W., Paijmans, J., Takahashi, K., Tostevin, F. and ten Wolde, P. R. (2014). The Berg-Purcell limit revisited. *Biophys. J.* **106**, 976-985. doi:10.1016/j.bpj.2013.12.030

Karginov, A. V., Ding, F., Kota, P., Dokholyan, N. V. and Hahn, K. M. (2010). Engineered allosteric activation of kinases in living cells. *Nat. Biotechnol.* **28**, 743-747. doi:10.1038/nbt.1639

Karginov, A. V., Tsygankov, D., Berginski, M., Chu, P.-H., Trudeau, E. D., Yi, J. J., Gomez, S., Elston, T. C. and Hahn, K. M. (2014). Dissecting motility signaling through activation of specific Src-effector complexes. *Nat. Chem. Biol.* **10**, 286-290. doi:10.1038/nchembio.1477

Kelley, L. C. and Weed, S. A. (2012). Cortactin is a substrate of activated Cdc42-associated kinase 1 (ACK1) during ligand-induced epidermal growth factor receptor downregulation. *PLoS ONE* **7**, e44363. doi:10.1371/journal.pone.0044363

Kennedy, M. J., Hughes, R. M., Peteya, L. A., Schwartz, J. W., Ehlers, M. D. and Tucker, C. L. (2010). Rapid blue-light-mediated induction of protein interactions in living cells. *Nat. Methods* **7**, 973-975. doi:10.1038/nmeth.1524

Kholodenko, B. N., Hoek, J. B. and Westerhoff, H. V. (2000). Why cytoplasmic signalling proteins should be recruited to cell membranes. *Trends Cell Biol.* **10**, 173-178. doi:10.1016/S0962-8924(00)01741-4

Krishnamurty, R., Brigham, J. L., Leonard, S. E., Ranjitkar, P., Larson, E. T., Dale, E. J., Merritt, E. A. and Maly, D. J. (2013). Active site profiling reveals coupling between domains in SRC-family kinases. *Nat. Chem. Biol.* **9**, 43-50. doi:10.1038/nchembio.1118

Kubiniok, P., Lavoie, H., Therrien, M. and Thibault, P. (2017). Time-resolved phosphoproteome analysis of paradoxical RAF activation reveals novel targets of ERK. *Mol. Cell. Proteomics* **16**, 663-679. doi:10.1074/mcp.M116.065128

Kumar, L. and Futschik, M. E. (2007). Mfuzz: a software package for soft clustering of microarray data. *Bioinformation* **2**, 5-7. doi:10.6026/97320630002005

Kuroiwa, M., Oneyama, C., Nada, S. and Okada, M. (2011). The guanine nucleotide exchange factor Arhgef5 plays crucial roles in Src-induced podosome formation. *J. Cell Sci.* **124**, 1726-1738. doi:10.1242/jcs.080291

Leroy, C., Fialin, C., Sirvent, A., Simon, V., Urbaeh, S., Poncet, J., Robert, B., Jouin, P. and Roche, S. (2009). Quantitative phosphoproteomics reveals a cluster of tyrosine kinases that mediates src invasive activity in advanced colon carcinoma cells. *Cancer Res.* **69**, 2279-2286. doi:10.1158/0008-5472.CAN-08-2354

Li, P., Banjade, S., Cheng, H. C., Kim, S., Chen, B., Guo, L., Llaguno, M., Hollingsworth, J. V., King, D. S., Banani, S. F. et al. (2012). Phase transitions in the assembly of multivalent signalling proteins. *Nature* **483**, 336-340. doi:10.1038/nature10879

Luo, W., Slebos, R. J., Hill, S., Li, M., Brábek, J., Amanchy, R., Chaerkady, R., Pandey, A., Ham, A. J. L. and Hanks, S. K. (2008). Global impact of oncogenic src on a phosphotyrosine proteome. *J. Proteome Res.* **7**, 3447-3460. doi:10.1021/pr800187n

Luxenburg, C., Parsons, J. T., Addadi, L. and Geiger, B. (2006). Involvement of the Src-cortactin pathway in podosome formation and turnover during polarization of cultured osteoclasts. *J. Cell Sci.* **119**, 4878-4888. doi:10.1242/jcs.03271

Mettlen, M., Platek, A., Van Der Smissen, P., Carpentier, S., Amyere, M., Lanzetti, L., de Diesbach, P., Tyteca, D. and Courtoy, P. J. (2006). Src triggers circular ruffling and macropinocytosis at the apical surface of polarized MDCK cells. *Traffic* **7**, 589-603. doi:10.1111/j.1600-0854.2006.00412.x

Moitrier, S., Pricoupenko, N., Kerjouan, A., Oddou, C., Destaing, O., Battistella, A., Silberzan, P. and Bonnet, I. (2019). Local light-activation of the Src oncoprotein in an epithelial monolayer promotes collective extrusion. *Commun. Phys.* **2**, 98. doi:10.1038/s42005-019-0198-5

Monteiro, P., Rossé, C., Castro-Castro, A., Irondelle, M., Lagoutte, E., Paul-Gilloteaux, P., Desnos, C., Formstecher, E., Darchen, F., Perrais, D. et al. (2013). Endosomal WASH and exocyst complexes control exocytosis of MT1-MMP at invadopodia. *J. Cell Biol.* **203**, 1063-1079. doi:10.1083/jcb.201306162

Olsen, J. V., Blagoev, B., Gnad, F., Macek, B., Kumar, C., Mortensen, P. and Mann, M. (2006). Global, In Vivo, and site-specific phosphorylation dynamics in signaling networks. *Cell* **127**, 635-648. doi:10.1016/j.cell.2006.09.026

Parsons, S. J. and Parsons, J. T. (2004). Src family kinases, key regulators of signal transduction. *Oncogene* **23**, 7906-7909. doi:10.1038/sj.onc.1208160

Pérez, Y., Maffei, M., Igea, A., Amata, I., Gairí, M., Nebreda, A. R., Bernadó, P. and Pons, M. (2013). Lipid binding by the Unique and SH3 domains of c-Src suggests a new regulatory mechanism. *Sci. Rep.* **3**, 1295. doi:10.1038/srep01295

Playford, M. P. and Schaller, M. D. (2004). The interplay between Src and integrins in normal and tumor biology. *Oncogene* **23**, 7928-7946. doi:10.1038/sj.onc.1208080

Rapali, P., Mitteau, R., Braun, C., Massoni-Laporte, A., Ünlü, C., Bataille, L., Arramon, F. S., Gygi, S. P. and McCusker, D. (2017). Scaffold-mediated gating of cdc42 signalling flux. *Elife* **6**, e25257. doi:10.7554/eLife.25257.016

Roskoski, R. Jr. (2015). Src protein-tyrosine kinase structure, mechanism, and small molecule inhibitors. *Pharmacol. Res.* **94**, 9-25. doi:10.1016/j.phrs.2015.01.003

Rossy, J., Owen, D. M., Williamson, D. J., Yang, Z. and Gaus, K. (2012). Conformational states of the kinase Lck regulate clustering in early T cell signaling. *Nat. Immunol.* **14**, 82-89. doi:10.1038/ni.2488

Sawada, Y., Tamada, M., Dubin-Thaler, B. J., Cherniavskaya, O., Sakai, R., Tanaka, S. and Sheetz, M. P. (2006). Force sensing by mechanical extension of the Src family kinase substrate p130Cas. *Cell* **127**, 1015-1026. doi:10.1016/j.cell.2006.09.044

Selvarajoo, K., Takada, Y., Gohda, J., Helmy, M., Akira, S., Tomita, M., Tsuchiya, M., Inoue, J. I. and Matsuo, K. (2008). Signaling flux redistribution at toll-like receptor pathway junctions. *PLoS ONE* **3**, e3430. doi:10.1371/journal.pone.0003430

Shaaya, M., Fauser, J., Zhurikhina, A, Conage-Pough, J. E., Huyot, V., Brennan, M., Flower, C. T., Matsche, J., Khan, S., Natarajan, V. et al. (2020). Light-regulated allosteric switch enables temporal and subcellular control of enzyme activity. *Elife* **9**, e60647. doi:10.7554/eLife.60647

Shah, K., Liu, Y., Deirmengian, C. and Shokat, K. M. (1997). Engineering unnatural nucleotide specificity for Rous sarcoma virus tyrosine kinase to uniquely label its direct substrates. *Proc. Natl. Acad. Sci. USA* **94**, 3565-3570. doi:10.1073/pnas.94.8.3565

Shannon, P., Markiel, A., Ozier, O., Baliga, N. S., Wang, J. T., Ramage, D., Amin, N., Schwikowski, B. and Ideker, T. (2003). Cytoscape: a software Environment for integrated models of biomolecular interaction networks. *Genome Res.* **13**, 2498-2504. doi:10.1101/gr.1239303

Smith, A. W., Huang, H. H., Endres, N. F., Rhodes, C. and Groves, J. T. (2016). Dynamic organization of myristoylated src in the live cell plasma membrane. *J. Phys. Chem. B* **120**, 867-876. doi:10.1021/acs.jpcb.5b08887

Spassov, D. S., Ruiz-Saenz, A., Piple, A. and Moasser, M. M. (2018). A dimerization function in the intrinsically disordered N-terminal region of Src. *Cell Rep.* **25**, 449-463.e4. doi:10.1016/j.celrep.2018.09.035

Steenblock, C., Heckel, T., Czupalla, C., Santo, A. I. E., Niehage, C., Sztacho, M. and Hoflack, B. (2014). The Cdc42 guanine nucleotide exchange factor FGD6 coordinates cell polarity and endosomal membrane recycling in osteoclasts. *J. Biol. Chem.* **289**, 18347-18359. doi:10.1074/jbc.M113.504894

Summy, J. M., Qian, Y., Jiang, B.-H., Guappone-Koay, A., Gatesman, A., Shi, X. and Flynn, D. C. (2003). The SH4-Unique-SH3-SH2 domains dictate specificity in signaling that differentiate c-Yes from c-Src. *J. Cell Sci.* **116**, 2585-2598. doi:10.1242/jcs.00466

Thomas, S. M., Soriano, P. and Imamoto, A. (1995). Specific and redundant roles of Src and Fyn in organizing the cytoskeleton. *Nature* **376**, 267-271. doi:10.1038/376267a0

Toettcher, J. E., Weiner, O. D. and Lim, W. A. (2013). Using optogenetics to interrogate the dynamic control of signal transmission by the Ras/Erk module. *Cell* **155**, 1422-1434. doi:10.1016/j.cell.2013.11.004

Valon, L., Etoc, F., Remorino, A., di Pietro, F., Morin, X., Dahan, M. and Coppey, M. (2015). Predictive spatiotemporal manipulation of signaling perturbations using optogenetics. *Biophys. J.* **109**, 1785-1797. doi:10.1016/j.bpj.2015.08.042

Vizcaíno, J. A., Csordas, A., Del-Toro, N., Dianes, J. A., Griss, J., Lavidas, I., Mayer, G., Perez-Riverol, Y., Reisinger, F., Ternent, T. et al. (2016). 2016 update of the PRIDE database and its related tools. *Nucleic Acids Res.* **44**, D447-D456. doi:10.1093/nar/gkw880

Vojtěchová, M., Šenigl, F., Šloncová, E. and Tuháčková, Z. (2006). Regulation of c-Src activity by the expression of wild-type v-Src and its kinase-dead double Y416F-K295N mutant. *Arch. Biochem. Biophys.* **455**, 136-143. doi:10.1016/j.abb.2006.09.011

Webb, D. J., Schroeder, M. J., Brame, C. J., Whitmore, L., Shabanowitz, J., Hunt, D. F. and Horwitz, A. R. (2005). Paxilin phosphorylation sites mapped by mass spectrometry. *J. Cell Sci.* **118**, 4925-4929. doi:10.1242/jcs.02563

Wieczorek, S., Combes, F., Lazar, C., Gianetto, Q. G., Gatto, L., Dorffer, A., Hesse, A. M., Couté, Y., Ferro, M., Bruley, C. et al. (2017). DAPAR & ProStaR: software to perform statistical analyses in quantitative discovery proteomics. *Bioinformatics* **33**, 135-136. doi:10.1093/bioinformatics/btw580

Wu, J.-C., Chen, Y.-C., Kuo, C.-T., Wenshin Yu, H., Chen, Y.-Q., Chiou, A. and Kuo, J.-C. (2016). Focal adhesion kinase-dependent focal adhesion recruitment of SH2 domains directs SRC into focal adhesions to regulate cell adhesion and migration. *Sci. Rep.* **5**, 18476. doi:10.1038/srep18476

Xue, Y., Liu, Z., Cao, J. and Re, J. (2011). Computational prediction of post-translational modification sites in proteins. In *Systems and Computational Biology - Molecular and Cellular Experimental Systems* (ed. N. -S. Yang). IntechOpen. e10.5772/18559. doi:10.5772/18559

Yeo, M. G., Partridge, M. A., Ezratty, E. J., Shen, Q., Gundersen, G. G. and Marcantonio, E. E. (2006). Src SH2 arginine 175 is required for cell motility: specific focal adhesion kinase targeting and focal adhesion assembly function. *Mol. Cell. Biol.* **26**, 4399-4409. doi:10.1128/MCB.01147-05

Young, M. A., Gonfloni, S., Superti-Furga, G., Roux, B. and Kuriyan, J. (2001). Dynamic coupling between the SH2 and SH3 domains of c-Src and Hck underlies their inactivation by C-Terminal tyrosine phosphorylation. *Cell* **105**, 115-126. doi:10.1016/S0092-8674(01)00301-4

Zhang, X., Moore, S. W., Iskratsch, T. and Sheetz, M. P. (2014). N-WASP-directed actin polymerization activates Cas phosphorylation and lamellipodium spreading. *J. Cell Sci.* **127**, 1394-1405. doi:10.1242/jcs.134692

Zisch, A. H., Pazzagli, C., Freeman, A. L., Schneller, M., Hadman, M., Smith, J. W., Ruoslahti, E. and Pasquale, E. B. (2000). Replacing two conserved tyrosines of the EphB2 receptor with glutamic acid prevents binding of SH2 domains without abrogating kinase activity and biological responses. *Oncogene* **19**, 177-187. doi:10.1038/sj.onc.1203304